Distribution Category
UC-20 b, d

LAWRENCE LIVERMORE LABORATORY
University of California/Livermore, California/94550

UCRL-50031-76

SUPERCONDUCTING MAGNET DEVELOPMENT PROGRAM ANNUAL REPORT; July 1975 Through September 1976

D. W. Deis
D. N. Cornish
J. P. Zbasnik
R. L. Nelson
S. J. Sackett
C. E. Taylor

MS. date: July 22, 1977

NOTICE
This report was prepared as an account of work sponsored by the United States Government. Neither the United States nor the United States Department of Energy, nor any of their employees, nor any of their contractors, subcontractors, or their employees, makes any warranty, express or implied, or assumes any legal liability or responsibility for the accuracy, completeness or usefulness of any information, apparatus, product or process disclosed, or represents that its use would not infringe privately owned rights.

DISTRIBUTION OF THIS DOCUMENT IS UNLIMITED

CONTENTS

Abstract 1

Introduction 1

Nb_3Sn Conductor Development 3

Introduction 3

Short-Sample Measurement Techniques 3

LLL/Airco Program Results 5

LLL/Supercon Program Results 13

LLL/Intermagnetics General Program Results 17

High-Field Cryogenic Tensile-Test Experiment 47

Magnet Development for MFTF 54

High-Field Test Facility 56

Summary 57

Acknowledgments 59

References 60

Publications 62

SUPERCONDUCTING MAGNET DEVELOPMENT PROGRAM ANNUAL REPORT
July 1975 Through September 1976

ABSTRACT

During FY76 Lawrence Livermore Laboratory (LLL) continued its development of niobium tin (Nb_3Sn) conductors and its design support for the mirror fusion test facility (MFTF) superconducting magnet. Three highlights came from within the Laboratory. LLL completed its cryogenic tensile-test apparatus for Nb_3Sn strain measurements. Over at MFTF, engineers ordered 2100 m of prototype material for a 1-m test coil. People at the high-field test facility (HFTF) released some components for fabrication; delivery was scheduled for early FY77. Outside LLL several subcontractors advanced Nb_3Sn manufacturing technology. One advance, in particular, improved conductor current densities at 12 T.

INTRODUCTION

LLL's magnet development program has three major objectives:

- Carry out design and development and support construction, commissioning, and operation of ongoing superconducting projects at LLL.
- Study technological requirements of most likely "next generation" machines, assist in conceptual designs, and carry out development programs so feasibility of the machines can be assured and preproject work limited to development and proving of prototypes.
- Play a useful role in superconducting magnet development for fusion applications and assist in reactor design studies.

At present, support work on MFTF is our principal effort in the first category. After the initial magnet design effort our main task has been development of the stabilized conductor and its subsequent qualification test as a relatively small (1-m-bore) solenoid. This work is well underway. Contracts have been placed with each of the four major superconductor manufacturers in the

USA for delivery of a prototype conductor to be evaluated at LLL. The total quantity on order will be sufficient, after addition of the copper (Cu) stabilizer, to fabricate the test coil. Contracts have also been placed with Supercon and Airco for developing alternative means of adding the Cu stabilizer to the conductor.

Other aspects of the MFTF work have been the development of stress analysis codes and more refined calculations of the stresses and displacements of the coil structure. This work has also been supported by an independent analysis by the Boeing Aircraft Company. The results of this work confirm that the proposed structural concept is sound and that the stresses and deflections are acceptable.

Several years ago the long-range need for mirror fusion magnets with peak fields in the range of 12 T was identified. Subsequently, in FY74, we initiated a program to develop multifilamentary Nb_3Sn to meet this requirement. This work, which is in the second category above, continued jointly between industry and LLL. The program is organized to take maximum advantage of industry's manufacturing capabilities and LLL's unique testing facilities. The manufacturers made significant progress in FY76 by solving production problems associated with extrusion conditions and by improving the achievable current density while maintaining production processes that will yield an economical conductor

The LLL effort resulted in the construction and testing of a 27-cm-bore coil that operates to its short-sample limit at 10 T with a conductor resistivity of less than 10^{-12} Ω-cm. Efforts were also successful in improving the sensitivity and reliability short-sample measuremerts. These measurements demonstrated that the critical-current-density goal of 10^4 A/cm^2 at 12 T (exclusive of Cu) can be achieved with present conductor configurations.

The 2.2×10^5-N load capacity tensile-test machine has been operating at room temperature, with cryogenic measurements planned for early FY77. This equipment is essential for evaluating the effects of strain on the prototype Nb_3Sn conductors. A part of the mechanical measurements program has been devoted to the characterization of foil-type strain gages for use at 4 K in fields up to 12 T. Calibration techniques and fixtures have been developed; the results to date are encouraging.

In FY76 the HFTF major project proposal was approved and construction of the cryostat initiated, with delivery scheduled for early FY77. Construction of the first two niobium-

titanium (Nb-Ti) backing coils and installation of the 100-litres/h Airco refrigerator obtained from the old LLL Baseball II-T experiment will occur in mid-FY77 so the system can be used for testing the MFTF test coil.

We have done continuing consulting work for LLL's reactor studies group on future mirror reactor concepts. Although this is a rather small effort on our part, it serves the important function of keeping development efforts generally directed toward appropriate long-range goals.

The rest of this report details the important points of progress made during FY76 on various program segments and indicates near-term work.

Nb_3Sn CONDUCTOR DEVELOPMENT

Introduction

When our Nb_3Sn development program began we established the general goal of a conductor capable of carrying 10 000 A at 12 T with an overall critical current density, J_c, of 10^4 A/cm^2 (exclusive of Cu). As work progressed this goal proved to be achievable and remained unchanged. When reliable cost-effective manufacturing procedures have been demonstrated for the prototype conductors, the program will proceed to coil tests at fields up to 12 T (see HFTF section).

During FY76 three outside contracts with manufacturers were active. Airco pursued the solid Nb filament-in-bronze approach while Supercon continued working on the bronze-in-hollow Nb filaments technique. In addition to these two efforts, which continued with only minor modifications since the program's inception, we funded Intermagnetics General to study the feasibility and advantages of a new processing method based on the high-Sn-bronze technique first studied in Japan.

The below information on the results of these three programs, which was compiled by LLL, relies heavily on reports submitted by each of the contractors and on the results of in-house LLL testing of material supplied by the contractors.

Short-Sample Measurement Techniques

During FY76 we attempted to increase the sensitivity of the short-sample testing apparatus so voltage levels corresponding to a resistivity of 10^{-12} Ω-cm could be measured. This was necessary for two reasons. First, the power dissipated in the windings of a large yin-yang magnet, for

programs such as MFTF or the fusion engineering test facility, would be on the order of several tens of watts for a conductor with a resistivity level of 10^{-12} Ω-cm. A high-sensitivity short-sample test, therefore, can be used to determine those processing schemes suitable for making low-loss magnets. Second, we have reason to suspect that when a brittle super-conductor such as Nb_3Sn undergoes a mechanical load, microcracks will form and cause small voltages to appear across the strained conductor. High-sensitivity measuring techniques are desired, therefore, for strain-effect measurements that accurately provide the responses of various conductors to mechanical strains. These data will enable us to predict magnet performance.

We took several steps to increase measurement sensitivity:

- The regulator was installed on the 10-kA power supply. This work began in FY75.
- Chopper-stabilized dc amplifiers were used to amplify the signals.
- Thermocouple emf's were eliminated by using continuous signal cables; solder joints were made only in the helium bath and at the instrument rack.
- Current junctions were lengthened to reduce joint heating.
- Samples were potted with RTV 732 to prevent sample motion due to Lorentz forces.

By making these improvements we were able to detect voltages between 50 and 100 nV, corresponding to a resistivity of ~10^{-12} Ω-cm for our conductors.

Short-sample measurements performed at a high sensitivity indicated that the samples supplied by Airco, for example, had an apparent resistivity of ~2×10^{-12} Ω-cm at zero current. Initially, we suspected defects in superconducting filaments, but it now appears that current transfer is responsible for this apparent resistive behavior.

In the low-field regions on the ends of the sample where current is injected, current is carried by the filaments near the outside of the conductor. In the high-field region, however, current is shared by more and more filaments as the critical current is reached. A certain length of conductor in the high-field region is needed to ensure that current is uniformly distributed throughout the filaments. Voltage taps should be positioned so they span the portion of the conductor in which current is uniformly distributed; otherwise the voltages measured will not be indicative of the superconducting components

and will be largely due to current flowing in the material between filaments.

M. N. Wilson[1] considered this problem. By approximating the multifilamentary composite as two concentric filaments, he calculated the transfer length. For conductors of our type, Wilson's expression reduces to

$$L \simeq 0.1\ D\ (P_t/P_o)^{1/2}\ , \qquad (1)$$

where D is the composite diameter, P_t is the transverse resistivity of the composite, and P_o is the desired or measured overall longitudinal resistivity.

For a bronze-matrix conductor, $P_t \simeq 10^{-6}$ Ω-cm. To measure P_o to the desired 10^{-12} Ω-cm levels, we need a transfer length of 100 D. If we assume that current transfer through the bronze regions is the controlling factor, the appropriate value for D is the diameter of one of the regions lined with tantalum (Ta), which is ~0.05 cm. Since the high-field region in the short-sample test magnet is only 5 cm long, it seems plausible to assume that the resistivity onset measured for all these conductors is due to currents flowing in the resistive portions of the conductor. The above considerations indicate that the present short-sample test facility is limited to measuring resistivities on the order of 10^{-11} Ω-cm. To measure resistivities at the 10^{-12} Ω-cm level in our large conductors, we would have to obtain a magnet with a uniform field region ~30 cm long.

LLL/Airco Program Results

Manufacturing

The details of the manufacturing approach used by Airco have been presented previously.[2-4] Basically, three extrusions are used to fabricate the final conductor. The first extrusion consists of Nb rods in bronze, the second is made up of first extrusion material inside a Ta-lined Cu sheath, and the third comprises second extrusion material inside a Cu sheath. Conductors with different current-carrying capacities are achieved by using the appropriate number of second extrusion elements in the third extrusion.

During this year, four types of material were produced:

- 1-kA material using Cu/10-wt%-Sn bronze.
- 3.5-kA material using Cu/10-wt%-Sn bronze.
- 1-kA material using Cu/13.5-wt%-Sn bronze.
- A 187-mm diam third-stage billet with the standard 3.5-kA configuration and Cu/10-wt% Sn was extruded to investigate scale-up problems.

The details of these conductor configurations appear in Table 1. The manufacturing procedures for these conductors follow:

1-kA, Cu/10-wt%-Sn Bronze. A 51-mm diam, 152-mm hex length, third-stage billet was packed with 19 hexes drawn from a second-stage billet extruded in FY75. Airco used the standard 1-kA configuration:

$$[19 \times (187 \times [19 \text{ Nb in Bz}])_{\text{Ta Cu}}]_{\text{Cu}}$$

with 34-area% Cu. Twenty test samples, each 1.68 mm × 5.00 mm × 1.2 m, were reacted and delivered to LLL. These consisted of one group of 10 samples (7 having a 50-mm twist pitch and 3 having no twist) reacted two days at 650°C and a second similar group reacted four days at 650°C. Figure 1 shows microsections of this conductor.

3.5-kA, Cu/10-wt%-Sn Bronze. A 101-mm diam, 213-mm hex length, third-stage billet was packed with 73 hexes drawn from second-stage billets extruded in FY75. Airco used the standard configuration previously used with 51-mm diam billets:

$$[73 \times (187 \times [19 \text{ Nb in Bz}])_{\text{Ta Cu}}]_{\text{Cu}}$$

with 34-area% Cu. Ten samples, each 3.12 mm × 9.40 mm × 1.2 m long, were reacted four days at 650°C and delivered to LLL. Seven samples had a twist pitch of 100 mm and three had no twist. Figure 2 has microsections of this conductor.

1-kA, Cu/13.5-wt%-Sn Bronze. Three 22-kg, Cu/13.5-wt% ingots were cast using a vacuum-induction melting furnace. After homogenization, Airco

Table 1. Typical conductor configurations for Airco samples (by bronze composition).

Properties	Cu/10-wt% Sn		Cu/13.5-wt% Sn
Configuration (kA)	1	3.5	1
Size (mm)	1.68 × 5.0	3.7 × 10.5	1.68 × 5.0
Filaments	67 507	259 369	102 163
Filament diam (μm)	4.5	4.5	4.1
Composition before reaction (area%):			
Cu	34.0	34.0	34.0
Ta	4.0	4.0	4.0
Nb	12.9	12.9	15.9
Bronze	49.1	49.1	46.1

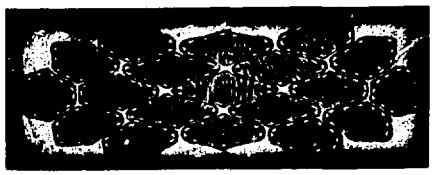

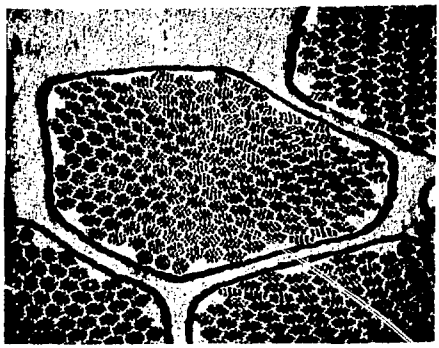

Fig. 1. Microsections of 1-kA Airco conductor manufactured with Cu/10-wt%-Sn bronze. Magnifications: 25X (top); 100X (bottom).

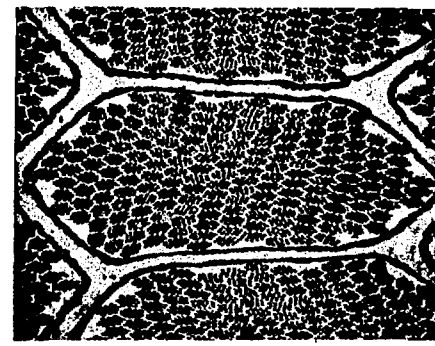

Fig. 2. Microsections of 3.5-kA Airco conductor manufactured with Cu/10-wt%-Sn bronze. Magnifications: 12.5X (top); 100X (bottom).

machined and drilled them to produce two 19-hole billets and one solid billet for filler stock, all 110-mm diam. The 19-hole billets were loaded with 118-mm-long Nb rods; the lids were electron-beam welded in a vacuum chamber. All three billets were extruded to 28.58-mm diam rods. The two 19-filament extrusions were 28.4-area% Nb.

Airco packed a 110-mm-diam, 203-mm hex-length second-stage billet with 283 hexes drawn from the 19-filament first-stage billets. They used solid filler stock to circularize the assembly inside the Ta liner. The Ta liner was 103-mm o.d. with a 1.59-mm wall. This billet was extruded to 28.6-mm diam and had a bronze-to-Nb ratio of 2.89/1. Microsections of this second extrusion at 0.686-mm diam appear in Fig. 3.

They packed a 75.7-mm diam, 152-mm hex-length third-stage billet with 19 hexes drawn from the second-stage billet; Cu fillers were used to circularize the assembly. This final configuration was

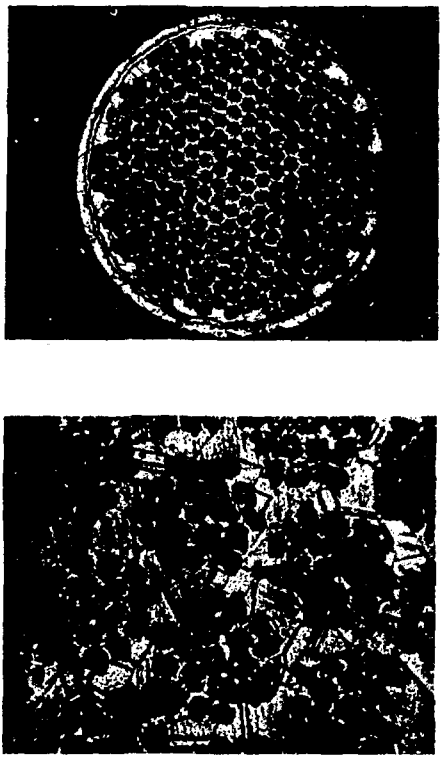

Fig. 3. Microsections of second extrusion material used to fabricate 1-kA, Cu/13.5-wt%-Sn bronze conductor. Magnifications: 110X (top); 1200X (bottom).

$$[19 \times (283 \times [19\text{Nb in Bz}])_{\text{Ta}}\ \text{Cu}]_{\text{Cu}}$$

with 34-area% Cu. This billet was extruded to 19.7-mm diam. The extruded rod was drawn to 4.11-mm wire, 20.6% reduction per draw, annealing every 3 draws. One portion of this wire was twisted, made rectangular in a turk's-head roll, then rectangular-die-drawn to a finished size of 1.68 × 5.00 mm with a 50-mm twist pitch. Another portion was processed similarly without twisting. Airco reacted seven twisted and three not-twisted samples, each 1.2-m long, for 72 h at 700°C and sent them to LLL. Figure 4 presents microsections of this conductor.

3.5-kA, Cu/10-wt%-Sn, 187-Diam Billet. Airco made this billet to investigate problems that might arise in scaling up toward production quantities. A 152-mm second-stage billet was packed with 187 hexes drawn from

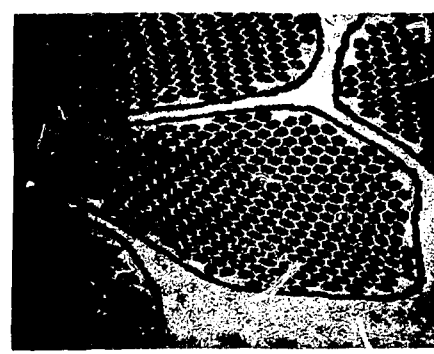

Fig. 4. Microsections of 1-kA, Cu/13.5-wt%-Sn conductor manufactured by Airco. Magnifications: 15X (top); 125X (bottom).

a 187-mm diam first-stage billet extruded in FY75. This billet, extruded to 38.18-mm diam, appeared perfect in cross-section. After annealing, the extrusion was drawn in three passes to 28.4-mm diam, annealed, then drawn in three more passes to 20.9-mm diam and annealed. At this point in the processing an examination revealed some breaks in the Ta barriers.

Since this type of problem had not been observed with smaller billets using Ta processed to the same specifications, Airco prepared another second-stage billet to make sure that all cleaning and assembly procedures were strictly adhered to. Similar problems were observed when this billet was extruded and drawn. At this point there is no satisfactory explanation for this problem, although work is continuing (as discussed later in this section).

To gain further information, and possibly produce some useful material, the rods produced were drawn to 17.9-mm hex and packed in a 187-mm diam, 305-mm hex-length third-stage billet. This billet was extruded to 50.8-mm diam, annealed, and drawn to 36.4-mm diam; it is being held in inventory at this size.

Short-Sample Results

Early in FY76 we performed short-sample tests on a series of *conductors with filament diameters ranging from 1.4 to 4.5 μm. The conductors, actually processed in FY75, are described in our FY75 progress report.*[5] The results of the short-sample tests were presented at the Sixth Symposium on Engineering Problems of Fusion Research.[4] A bronze containing 10-wt% Sn was used in these conductors.

Figure 5, which summarizes the results of this work, plots critical currents of the various conductors at 12 T and 4.2 K against the time of heat treatment at 650°C. The conductors all have the same external dimensions and Nb area. The data for the 1.4-μm filaments show that their performance severely degraded. We had difficulties when processing this material; microscopy showed some filament breakage and some broken Ta barriers.

These experiments indicated that higher critical currents could be

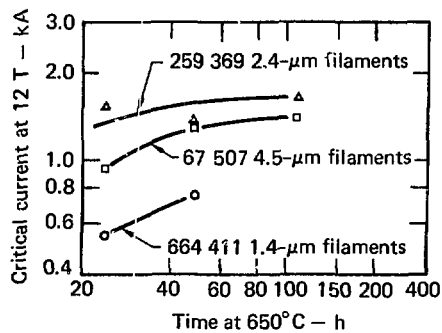

Fig. 5. Short-sample test results on Airco conductor samples with various filament diameters for different heat treatments.

achieved by using smaller filament diameters. The increase is quite small, however, and the cost and problems of the extra drawing and annealing steps offset the gains from the increase in critical current. We expect that the behavior of conductors processed from 13-wt%-Sn bronze will be similar; future development efforts will therefore be limited to conductors having 4.5-μm or 5-μm-diam filaments.

Short-sample *testing at higher sensitivity showed that, similar to* work done in FY75 at low sensitivity, large cross-sectional area conductors can be processed and that critical current is proportional to the number of filaments. This work was reported at the 1976 Applied Superconductivity Conference[6]; the data appear in Fig. 6. The conductors used here were all based on a 10-wt%-Sn bronze.

In FY76, development work began on *conductors based on a 13.5-wt%-Sn bronze*. Several considerations led us to believe that a conductor with a critical current substantially higher than that for the 10-wt%-bronze matrix conductors could be fabricated. This work was reported at the 1976 Applied Superconductivity Conference.[6]

Figure 7 shows the short-sample characteristics of a "1,000-A-size" conductor. The details of this conductor can be found in Table 1, which appears at the beginning of this section. By comparing the data in Fig. 7 with that in Fig. 6 one can see that the 13.5-wt%-Sn conductor carries 70% more current than a 10-wt%-Sn conductor of the same size. According to Airco estimates of the Nb_3Sn areas in the various conductors, the 13.5-wt%-Sn conductors contain 40% more Nb_3Sn than those with 10-wt% Sn. The observed 70% increase in critical current therefore implies that the Nb_3Sn current density in the 13.5-wt%-Sn material is higher than that for the 10-wt%-Sn bronze.

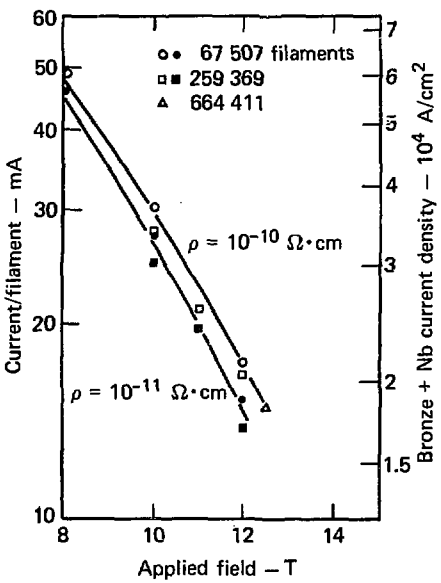

Fig. 6. Short-sample test results on Airco conductors containing different numbers of filaments heat treated at 650°C and 100 h.

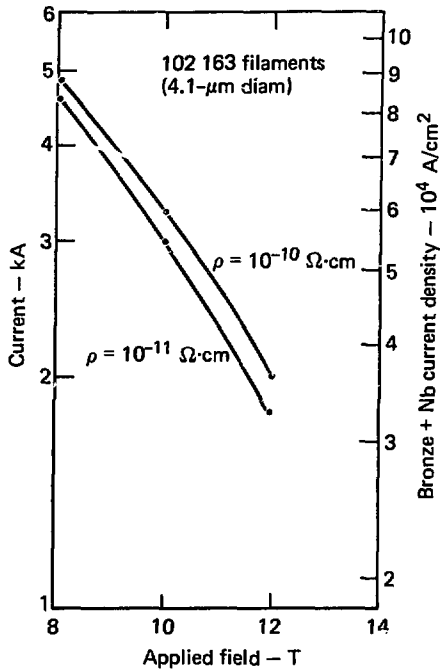

Fig. 7. Short-sample test results for Cu/13.5-wt%-Sn bronze Airco 1-kA conductor, 1.68 × 5.1 mm, heat treated at 700°C and 72 h.

Coil Tests

In early FY76 we wound a coil from prereacted multifilamentary Nb_3Sn conductor purchased from Airco. The conductor, which was 1.7 mm × 5.0 mm in cross-section, contained 67 507 filaments and was 325 m long. We received it on a 56-cm diam spool, on which it had been reacted. The conductor was spirally wrapped with Nomex tape and wound onto a 27.5-cm diam coil form. The coil, complete with current and diagnostic leads, is in Fig. 8. We inserted this coil in the bore of a Nb-Ti solenoid that provided a backing field of up to 5 T. The coil performance data in Fig. 9 show that, after some initial training, the Nb_3Sn test coil produced a 5-T field increment to the 5-T background field and reached the short-sample limit of 10 T. We presented this work at the 1975 Cryogenic Engineering Conference.[7]

In the completed coil the conductor has a maximum fiber strain of ~0.3%. When the coil was energized, magnetic loading may have added an additional

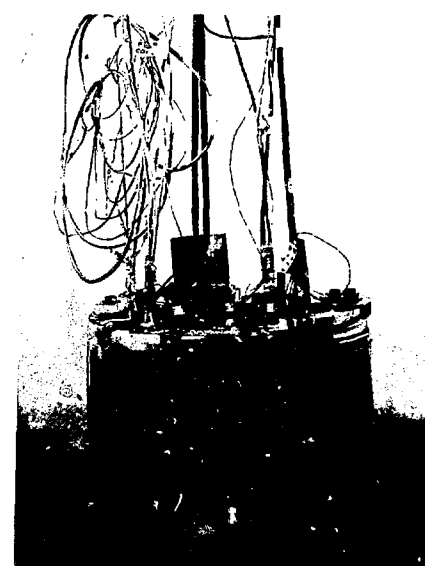

Fig. 8. Nb_3Sn test coil wound with 1-kA Airco conductor using Cu/10-wt%-Sn. The coil dimensions are 27.5 cm i.d., 32.8 cm o.d., and 13.3 cm long.

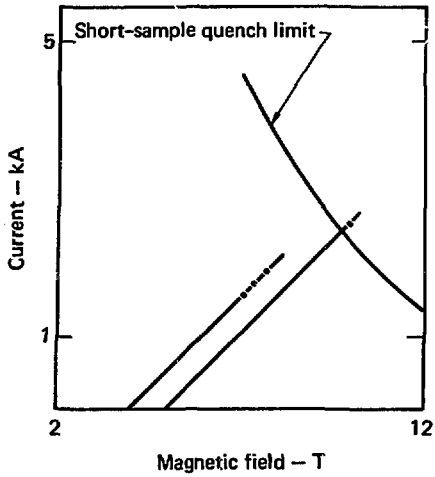

Fig. 9. Test results for Nb_3Sn coil shown in Fig. 8. Peak field was 10 T.

0.1% tensile strain. It is encouraging that the coil performed to the short-sample limit with this strain. Unfortunately, however, spurious voltages generated by noise on the power supplies prevented us from measuring a resistivity less than 10^{-10} Ω-cm. This precluded any measurement of the resistive transition.

We retested the coil recently, using improved power supplies and diagnostic equipment. As mentioned earlier a regulator was installed on the 10-kA power supply. This supply powered the Nb_3Sn test coil. We obtained a regulated power supply, capable of supplying 3000 A at 15 V, from the Baseball II-T project and installed it to power the Nb-Ti solenoid that provides the background field. An identical power supply, obtained at the same time, can be connected when needed.

In the latest series of tests premature quenching of the system, primarily the Nb-Ti solenoid, limited the performance of the Nb_3Sn coil to 2100 A and 8.5 T. Prior to the quenches, however, we were able to determine that the resistivity was less than 10^{-12} Ω-cm. At this field and current, on the other hand, short-sample tests indicate that the conductor has a resistivity of $\sim 3 \times 10^{-12}$ Ω-cm. These latest coil test results are incomplete in the sense that we were unable to trace out the resistive transition in the coil. They indicate, however, that current transfer effects in our short-sample apparatus underestimate the conductor performance at high sensitivities and limit the sensitivity that can be obtained.

Mechanical Properties Measurements

We performed a fairly extensive study of the room temperature mechanical properties of the various Airco conductors in FY76 before beginning similar measurements at 4.2 K in FY77. The one parameter that showed interesting behavior was the strain-to-failure, ε_f. Measurements made early in FY76 on the 1-kA conductor used in constructing the solenoid test coil gave

values of ε_f of ~10 to 15%, indicating good overall ductility. On the other hand, when samples manufactured more recently were measured, values of 1 to 2% were obtained, indicating poor ductility.

Since at first these results were rather puzzling, Airco checked out several possible explanations. First, measurements of ε_f were made on all the individual materials used in the conductor manufacturing after they were given a typical heat treatment. In all cases the materials exhibited good ductility. Second, chemical analysis of conductor samples with both high and low values of ε_f were made. They found no differences in impurities or impurity concentrations of any significance. Electron microscopy results of fracture surfaces showed that the Cu, bronze, Nb, and Ta exhibited microductility in all cases.

After the above results were obtained Airco made a series of tests on conductors given various heat treatments designed to vary the volume fraction of Nb_3Sn present. Previous work by Old and Charlesworth[8] at the A.E.R.E. Harwell Laboratories had shown that if the volume fraction of Nb_3Sn exceeded some critical value in the neighborhood of 15%, the entire conductor would exhibit brittle properties. By comparing ε_f and Nb_3Sn fraction in various conductors we were able to conclude that our observations were consistent in most all respects with those of Old and Charlesworth.

Although Nb_3Sn volume fraction is probably predominant in determining ε_f we expect that such parameters as filament spacing, filament-to-matrix bond strength, and the presence of unreacted Nb would also contribute.

Continuing Work

Current work at Airco includes

- Ta-barrier processing techniques.
- Fabrication of a short length of Rutherford-type cable from strands using 13.5-wt%-Sn bronze.
- Processing of high (>3) aspect ratio conductors.

LLL/Supercon Program Results

Manufacturing

Supercon has been pursuing a manufacturing approach for containing bronze in Nb tubes, which are in a Cu matrix. In some cases Nb/1-wt%-zirconium (Zr) tubes have been used (as discussed below). In this geometry the tube serves both as Nb source for the Nb_3Sn and as a diffusion barrier. This eliminates the need for Ta barriers.

During the initial phases of this work Nb/1-wt%-Zr tubes were used on

the assumptions that the Zr would enhance the critical current density and, because of its finer grain structure as compared with Nb, Zr would lead to a smoother interface with the bronze (which would be beneficial for obtaining more uniform Nb_3Sn layer growth along the length of a filament). As such, a number of first-extrusion billets were processed without any problems. However, when this material was rebundled and extruded for a second time, severe filament breakage was encountered. After a subsequent series of experiments Supercon determined that only by lowering both the extrusion ratio and temperature could satisfactory material be produced. This result, and the critical-current results discussed below, led us to abandon the Nb/1-wt%-Zr tube material in favor of pure Nb.

From the material produced during the above extrusion studies and from the parallel Nb tube-extrusion tests, Supercon delivered several different types of material to LLL for short-sample testing (see Table 2). The samples are from second extrusions using 51-mm-diam billets and Cu/13-wt%-Sn bronze. Figures 10 and 11 show microsections of the Nb and Nb/1-wt%-Zr material.

Short-Sample Results

A series of samples produced by Supercon were tested in FY76. One objective of these tests was to determine the relative merits of Nb vs Nb/1-wt%-Zr tubular filaments; a second was to do some preliminary work on the effect of filament diameter on critical current. Table 2 presents the characteristics of the conductor samples.

Table 2. Supercon conductor samples.

Size (mm)	Bronze + Nb area (cm^2)	Filaments	Filament diam (μm)	Tube material	Heat treatment Time (h)	Heat treatment Temp (°C)
2.7 (diam)	0.020	14 400	13	Nb	36	750
2.7 (diam)	0.020	14 400	13	Nb	120	650
5.3 (diam)	0.074	14 400	26	Nb	36	750
5.3 (diam)	0.074	14 400	26	Nb	120	650
2.7 (diam)	0.074	9 800	16	Nb/1-wt% Zr	30	750
6.1 (diam)	0.108	9 800	37	Nb/1-wt% Zr	30	750
1.7 × 5.3	0.033	14 400	17	Nb	36	750
1.7 × 5.3	0.035	9 800	21	Nb/1-wt% Zr	36	750

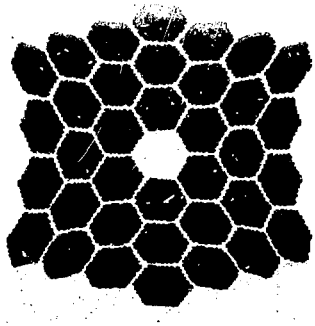

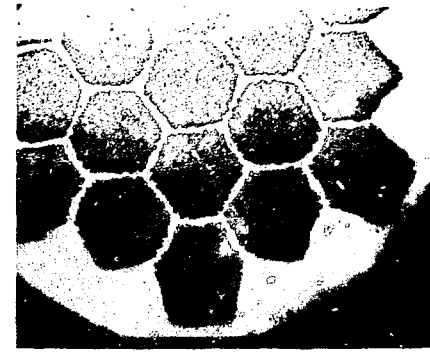

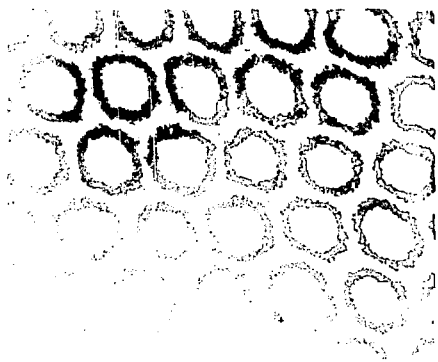

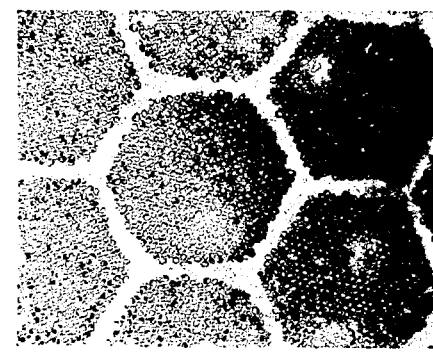

Fig. 10. Microsections of double-extrusion Supercon conductor using Nb tubular filaments. Magnifications: 15X (top); 500X (bottom).

Fig. 11. Microsections of double-extrusion Supercon conductor using Nb/1-wt%-Zr tubular filaments. Magnifications: 50X (top); 100X (bottom).

The results of these investigations appear in Figs. 12 and 13. The Cu areas were excluded in the calculation of current density for these conductors. The data in Fig. 12 show that for pure Nb material heat-treated at 650°C for 120 h, initial current density was higher for the conductor with 13-μm-diam filament material than that with 26-μm-diam material. For the samples heat treated at 750°C for 26 h, however, the reverse was found: smaller filaments had a lower critical current density than larger ones. The optimum filament diameter for Nb filaments heat-treated at 650°C for 120 h was <26 μm; for a 36-h heat treatment at 750°C, the optimum was

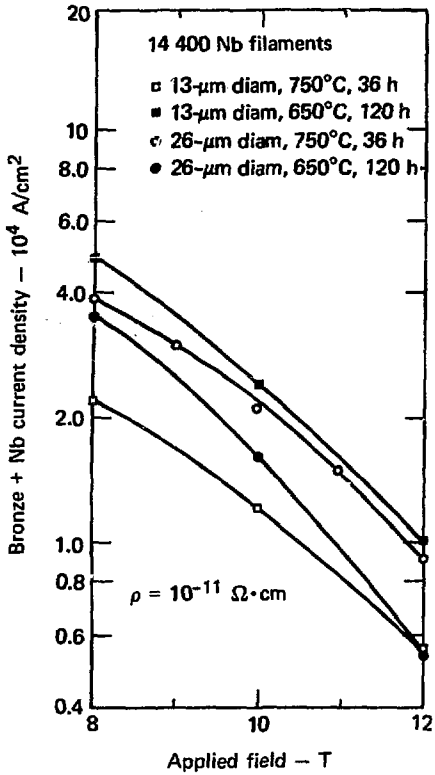

Fig. 12. Short-sample test results for Nb-filament Supercon conductors with various heat treatments.

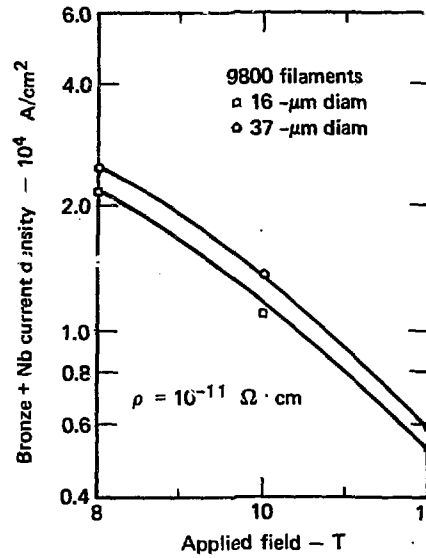

Fig. 13. Short-sample test results for Nb/1-wt%-Zr filament Supercon conductors heat treated at 750°C and 30 h.

>13 μm. Tests will be done in the future to determine the optimum values.

Fig. 13 presents the short-sample data for conductors with Nb/1-wt%-Zr filaments heat-treated at 750°C for 30 h. These results also indicate that the optimum filament diameter for these conductors is >16 μm.

These investigations, which were reported at the 1976 Applied Superconductivity Conference,[6] demonstrated that conductors with critical current densities near the goal of 10^4 A/cm^2 at 12 T and 4.2 K can be made using the bronze-filled tube approach. This work also shows that conductors with Nb/1-wt%-Zr tubes have current densities probably lower than those for pure Nb tubes. Since the material with Nb/1-wt%-Zr tubes is harder to process than that with pure Nb tubes, there is no advantage to using Nb/1-wt%-Zr material. Future work will involve only pure Nb filaments.

Mechanical Properties Measurements

For comparison with the Airco results we tested the two rectangular samples listed in Table 2 to determine their ε_f at room temperature. For both of these samples a 6.7% elongation at failure was measured. Estimates of the vol% of Nb_3Sn were 6% for the Nb and 3% for the Nb/1-wt%-Zr material. The relatively high elongation observed would seem to be consistent with these relatively low Nb_3Sn volume fractions. Further measurements on other samples may indicate whether there are any advantages (or disadvantages) of tube geometry vs solid-filament geometry as far as mechanical properties are concerned.

Continuing Work

Current work at Supercon includes

- Fabrication and processing of four different 51-mm-diam second-extrusion billets using Nb tubes to investigate the effect of filament size and heat treatment on overall J_c.
- Fabrication and processing of a 213-mm-diam second-extrusion billet with a nominal 3500 A at 12 T rating at 7.6 × 7.6 mm size.

LLL/Intermagnetics General Program Results

Introduction

During FY75 we funded Intermagnetics General (IGC) to investigate the potential of a new manufacturing technique. This technique, called the high-Sn bronze process because it uses a Cu-Sn alloy containing ~85-wt% Sn, was first studied by Hashimoto.[9] At the start of the program some of the potential advantages attributed to this process were

- A greater quantity of Sn may be included in the reaction matrix. To be workable, Cu-rich bronzes cannot exceed 15-wt% Sn. Beyond this concentration bronze becomes a two-phased alloy consisting of α-bronze and the brittle ε phase. The result of the increased Sn concentration should be an increased overall composite current density, a reduction in the quantity of materials needed for a given ampere-metre of conductor, and an increase in the ampere-metre yield of the billet. These factors should yield a lower conductor fabrication cost and longer conductor lengths per billet.

- As demonstrated by Hashimoto *et al.*[9] the composites consisting of pure Cu, Sn/20-wt% Cu, and Nb may be drawn to their final diameter without a single anneal. The replacement of the α-bronze matrix with such a two-element matrix would eliminate the annealing schedule needed to reduce α-bronze composites to their final diameter. The net result should not only be a reduction in conductor cost but also a time decrease from billet construction to final conductor.
- Casting of α-bronze to form the elements for billet preparation would be replaced by the casting of the lower melting point Sn-rich alloys and fabrication of pure Cu elements. Here as well there is a potential cost savings since oxygen-free, high-conductivity (OFHC) Cu is more easily worked and the cost of casting Sn-rich alloys is less than that for α-bronze.

The IGC program was created to investigate, and thus help define, the potential of this method as compared with conventionally processed material. Some of the questions still needed to be answered were

- The ability to extrude composites consisting of Cu, Nb, Sn-rich alloy, and Ta. Pressures required for the conventional extrusion of Cu-based composites at room temperature are prohibitively high. Billet preheating to at least 550°C, which is generally applied to reduce these pressures, is significantly above the melting point of Sn (232°C) and would therefore disrupt the composite. A reasonable alternative might be found in room-temperature hydrostatic extrusion. Although reductions of 15/1 in area have been accomplished on OFHC Cu by cold hydrostatic extrusion, we must examine the effect of billet heating resulting from dissipation of the energy of plastic deformation during cold hydrostatic extrusion.
- The feasibility and procedure for producing the elements for billet stacking. These elements include hexagonal rods of the Sn-rich alloy. The drawing of pure Sn or Sn-rich alloy by itself is made difficult by the softness of pure Sn and the brittleness of Sn-Cu alloys. The amount of jacketing with Cu and the soundness of the drawn jacketed rods must be determined.

- The soundness of the Sn or Sn-alloy filaments after reduction to the final diameter must be established.
- The size and distribution of Sn-alloy filaments that will ensure a sound conductor and uniform diffusion must be determined. Limitations on the size of these filaments may result from development of Kirkendall voids that should not engulf groups of Nb filaments. As Sn and Cu interdiffuse prior to reaction, non-α-bronze phases necessarily form. Previous investigations suggest that Nb_3Sn is not formed when Nb filaments are in contact with Cu-Sn alloys other than α-bronze. The extent of their growth is therefore an important consideration in the design of an optimal conductor.

The cost and availability of hydrostatic extrusion facilities and their impact on overall conductor fabrication cost and feasibility must be established.

Background

This section discusses hydrostatic extrusion as it applies generally to superconducting composites and specifically to the new type of conductor being considered. We also discuss some aspects of the diffusion of Sn in Cu-Sn alloys specifically relevant to this problem.

Hydrostatic Extrusion. Figure 14 illustrates the fundamental difference between hydrostatic and conventional direct extrusion. Instead of being in contact with the container walls as in conventional extrusion, the billet in hydrostatic extrusion is supported by a fluid over all surfaces except those in contact with the die. The extrusion driving force in hydrostatic extrusion is not provided

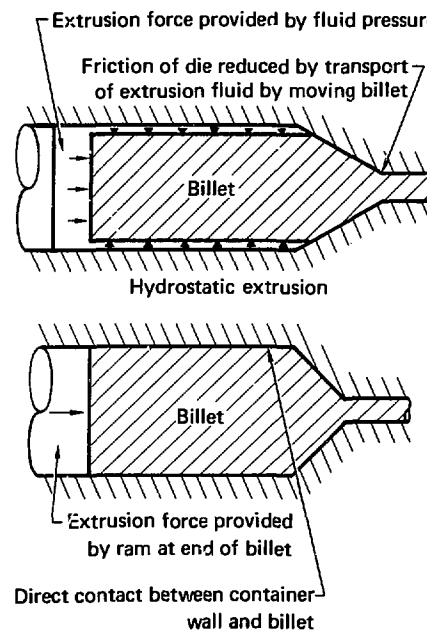

Fig. 14. Hydrostatic and conventional extrusion processes.

directly to the end of the billet as in conventional extrusion. Instead, the force is applied to the billet as pressure applied over all surfaces exposed to the hydrostatic fluid. This mode of applying the extrusion driving force has at least three fundamental advantages.

- Hydrostatic pressure considerably enhances the ductility of the material being extruded. This aspect of metals, which has been extensively investigated by Bridgeman[10] and others, results from the prevention of pores and microcracks involved in the mechanism of fracture. Consequently a hydrostatic process permits the extrusion of materials too brittle to be extruded conventionally. There is, therefore, much greater assurance of producing a sound extrusion of Cu or Cu-alloy composites at room temperature by hydrostatic extrusion than by conventional extrusion.
- The billet is supported by a fluid in the extrusion container rather than by a container wall. This eliminates an important component of friction, which considerably reduces the extrusion pressure necessary for a given conductor. This fact is particularly important to the composites in question, which contain low melting-temperature alloys of Sn. The temperature rises occurring in these composites during extrusion are roughly proportional to the work expended or pressures. Peak temperature will undoubtedly be the factor limiting the permissible reduction ratios.
- When fluid is continually in contact with the billet up to the die as it is in hydrostatic extrusion, the fluid could possibly be carried into the die when the billet velocity exceeds a critical value. This situation, often referred to as hydrodynamic lubrication, reduces die friction and, consequently, reduces extrusion pressures. As will be discussed later the existence of a lubricating film in the die allows a greater range of die angle. Thus we have greater possibilities for reducing undesirable effects observed in conventional extrusion (such as the piping defect and distortion[11]).

Hydrostatic extrusion's ability to reduce Cu at room temperatures is essential to the proposed conductor

because of the low melting point of Sn-rich Cu-Sn alloys (solidus: 227°C). Even with hydrostatic extrusion, however, there is concern over billet heating occurring as a result of dissipation of the work of deformation. If the reduction ratio is high enough the Sn phase may acquire the latent heat necessary to cause melting. The reduction ratio necessary to bring about melting and the effect of such melting on the integrity of the composite will be established in this study. If the limiting reduction is that at which melting occurs, such a factor will be important in establishing the economics of the process.

With the increasing awareness of its unique capabilities, cold hydrostatic extrusion has become a fully commercial method of reducing production-size billets to rod and wire. ASEA (Alumanna Svenska Electriska Aktiebolaget) of Sweden now offers a range of production hydrostatic-extrusion presses extending up to a capability of 2000 MPa with a container that may accommodate a billet 18-cm diam and 120-cm long (31 000 cm^3).[12,13] With a capability of 20 cycles per hour this hydrostatic extrusion press compares in production rate with a conventional extrusion press. A major production application of hydrostatic extrusion of large billets is the manufacture of Cu-clad aluminum wire. For example, the National Standard Company in Scotland produces such wire using a 3.6 $\times 10^6$-kg extrusion press built by ASEA.[13] In addition to this there are other large ASEA hydrostatic extrusion presses in Japan, Holland, and Sweden. The United States has a number of experimental extrusion presses of relatively small size (listed in Table 3). Battelle (Columbus, Ohio) is currently investigating the feasibility and cost of converting existing conventional presses to hydrostatic presses.

In addition to the extrusion of large-diameter billets there are several schemes for the reduction of rod and wire either by a purely hydrostatic extrusion or by a combination of hydrostatic extrusion and tensile forces on the exiting wire (augmented hydrostatic extrusion).[14,15] An example of a technique for wire drawing that relies on continuous hydrostatic extrusion is that presently under development at Western Electric Company.[16] Their machine (Fig. 15) provides a continuous track loop. As can be seen, the four continuous tracks provide four chamber segments through which the rod is extruded. Rather than gripping the rod directly, a viscous liquid (e.g., polyethylene) transfers pressure from the chamber segments to the rod. With traction also provided in this manner the rod is drawn into a high-pressure region

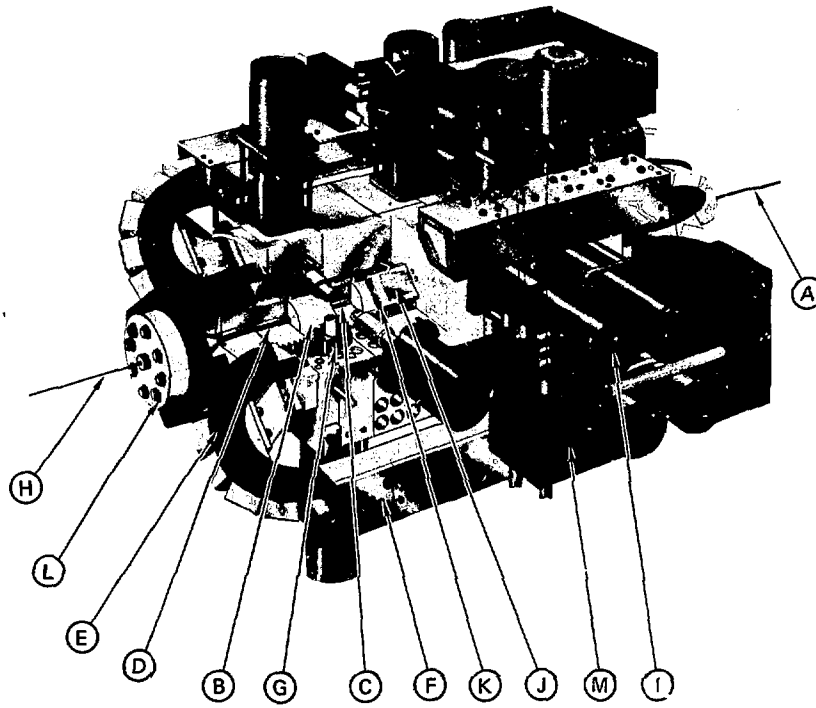

A. Wire rod
B. *Chamber segments*
C. Extrusion die
D. Die stem
E. Track loop
F. Straight track
G. Pinion gear
H. Extruded wire
I. Hydraulic motor & gear reducer
J. Fluid-pressure pad
K. Cooling-water passage
L. Load cell
M. *Hydraulic-fluid manifold*

Fig. 15. Mod-III endless-chamber extruder. *This continuous hydrostatic* extruder is under development at Western Electric Company (Ref. 16).

Table 3. Some hydrostatic-extrusion facilities in the U.S.

Location	Billet diam (cm)	Billet length (cm)	Pressure (MPa)	Comment
Westinghouse R&D Center (Pittsburg, Pennsylvania)	3.8	20	1034	
	2.54	20	2067	
Battelle Laboratory (Columbus, Ohio)	12.7	40.6	1724	Converted 2.2×10^7-N conventional press
Battelle Laboratory	6	30.5	2067	
Stanford University (Palo Alto, California)	1.91	20	1724	
	0.95	20	3448	
Be[illegible] Weapons Laboratory (Watervliet Arsenal, Watervliet, New York)	2.54	15.24	2067	

further in the machine where diameter reduction is accomplished on the rod. Conventional wire-drawing techniques involving tensile forces pulling the wire through the die are capable of only 10 through 30% reduction in area because of the limited tensile strength of metals. This machine at Western Electric, on the other hand, reduces aluminum (Al) rod to wire with a reduction ratio of 325 and a rod speed of 3 fpm. Having only a 0.79-cm bore in the pressure chamber, this machine cannot be used for either billets or for the rod resulting from the extrusion of a 20- to 25-cm diam billet.

Large extrusion presses such as those produced by ASEA represent a significant capital investment on the order of tens of millions of dollars. To our knowledge, there is no American company contemplating the purchase of such a press in the near future.

The cold hydrostatic extrusion of Cu, Al, and other materials has been extensively studied. Figure 16 shows the necessary extrusion pressure as a function of reduction ratio for Cu and several other materials. In a manner analogous to conventional extrusion the analytic expression relating extrusion pressure to reduction ratio for hydrostatic extrusion is

$$P = A \ln R + B, \qquad (2)$$

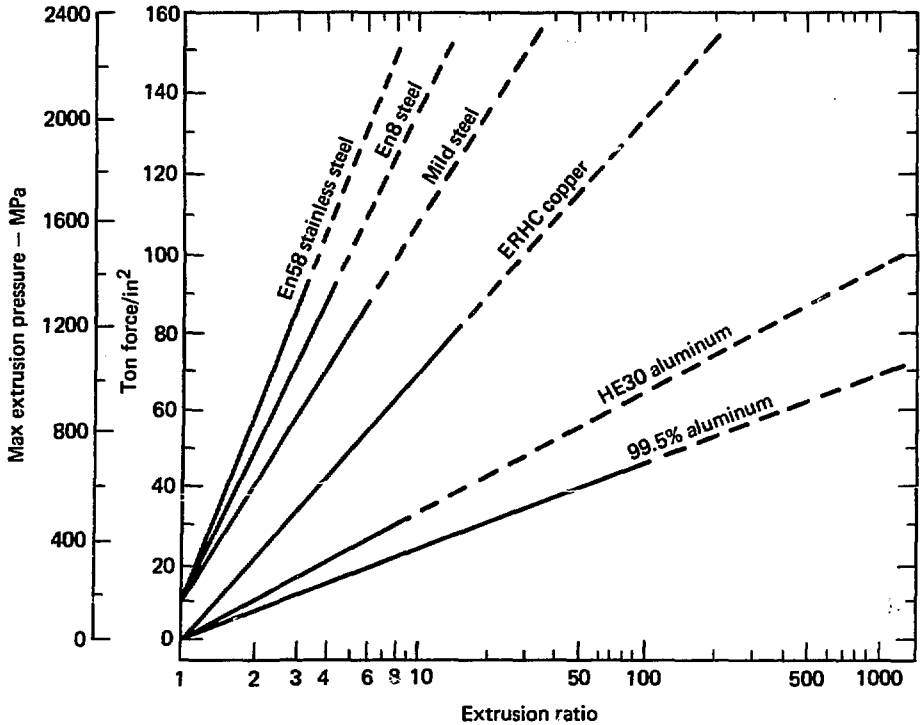

Fig. 16. Examples of reduction obtainable by hydrostatic extrusion of round billets through a single circular die.

where P is the pressure, R is the reduction ratio, and the constants A and B depend on such factors as die angle, condition of friction in the die, and billet diameter.[11]

An important factor determining extrusion pressure is die design. Dies commonly used in practice are conical, with a cone angle chosen according to material properties, reduction ratio, and condition of friction prevailing at the die. For a given set of conditions (such as coefficient of friction at the die, material yield stress, and reduction ratio) there is a die angle that corresponds to a minimum in the extrusion force. In conventional extrusion the optimal die angle usually increases with increasing extrusion ratio and coefficient of friction. This feature has been demonstrated analytically in the text of Avitzur[11] and is expressed in a

formula relating driving stress to reduction ratio, die angle, and coefficient of friction.

Another factor determining extrusion pressure is the strain rate of the material being deformed. Even without strain hardening, deformation stresses generally increase with increasing strain rate.

A third factor in determining extrusion pressure that is particularly important to the process of hydrostatic extrusion is the possibility of hydrodynamic lubrication. This phenomenon, characterized by a continuous film of lubricant separating the billet from the die, occurs when the lubricant is sufficiently viscous, the velocity of material at the die is sufficiently high, and the extruded rod diameter is sufficiently small.

Hydrodynamic lubrication is more readily maintained in cold hydrostatic extrusion than in conventional warm or hot extrusion because of the stability of the lubricant at lower temperatures and the greater availability of the extrusion fluid under pressure as a die lubricant. Since the velocity of the material at the die generally increases with decreasing die angle for a given reduction ratio and since a minimum velocity is necessary to maintain hydrodynamic lubrication, the phenomenon is more likely associated with smaller die angles.

Hydrodynamic lubrication provides an important benefit to the extrusion of superconducting composites. As mentioned earlier the optimal die angle increases with increasing friction and extrusion ratio. At higher reduction ratios (e.g., 20/1) the extrusion pressure increases rapidly as one reduces die angle from the optimal value. The defects that occur near the ends of the extruded rod, such as distortion of the filament pattern and the piping defect (Fig. 17), are more severe as one increases the die angle. In conventional extrusion we are thus forced by the necessity of reducing extrusion pressure to choose a die angle that results in a more extensive region of the extruded rod characterized by defects. In a typical extrusion of bronze-Nb composite, up to 20% of the extruded rod must be discarded because of these defects. The existence of hydrodynamic lubrication during hydrostatic extrusion reduces friction and therefore reduces the optimal die cone angle. We thus have good reason to believe that billet discard will be reduced when conventional warm extrusion is replaced by cold hydrostatic extrusion of Cu-based composite billets.

Because of the existence of a low melting-temperature material in the

Fig. 17a. Example of the piping defect occurring during the conventional extrusion of a composite billet.

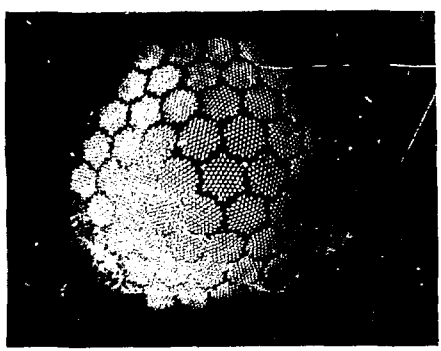

Fig. 17b. Distortion of filament pattern occurring near the ends of the extruded rod.

composite billets of the proposed approach, there is concern over temperature rises resulting from the dissipation of the work of deformation. We must thus understand the effect of extrusion rate, heat conduction, and billet size on the peak temperature reached by the billet. The analysis of the thermal problem during extrusion is complicated by the simultaneous process of heat generation, transport of heat by moving material, and conduction of heat by thermal diffusion. Several investigations, however, have made progress in estimating heating effects during conventional and hydrostatic extrusion through conical dies. By using a finite element technique for the calculation of temperature and by determining the velocity and strain fields from a viscoplasticity experiment, Altan and Kobayashi[17] calculated non-steady state temperatures along the length and cross section of the billet at particular stages of the extrusion.

Using a similar means of analysis, Guha and Lengyel[18] calculated the temperature distribution in a billet during hydrostatic extrusion/drawing. Carrying out their calculations by assuming properties of high-conductivity Cu, they theoretically established some interesting aspects of temperature distribution during the extrusion process. Figure 18 reproduces their curves. It shows the variation of temperature over the cross section of the extrusion product at the die exit for several values of coefficient of friction and billet velocity. As one would expect, there is peaking in the temperature at the surface of the extruded rod. However, reducing the extrusion speed not only reduces the average temperature achieved but also tends to eliminate the peak in

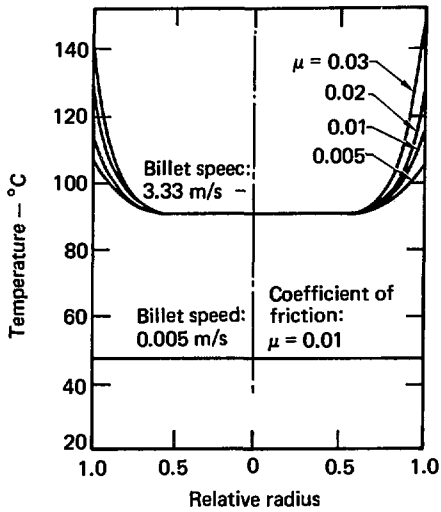

Fig. 18. Calculated curves of temperature variation over cross section of extrusion product at die exit for several values of coefficient of friction and billet velocity.

temperature at the surface resulting from friction. Figure 19, which shows their curves of temperature rise of the material as a function of the progress of the extrusions, indicates that a steady-state temperature is rapidly achieved during the extrusion process. Temperature measurements of Singer and Al-Samarrai[19] on materials exiting an extrusion die confirm the qualitative temperature variation theoretically predicted by Guha and Lengyel.[18] Figure 20, which shows Singer and Al-Samarrai measurements of the rise in emergent temperature as a function of ram travel for lead (Pb), demonstrates the temperature plateau reached early in the extrusion as well as the variation of this steady-state temperature with extrusion speed. Figure 21 shows their curves for the rise in emergent temperature as a function of ram travel for Sn billets subjected to various reduction ratios. The variation of temperature with extrusion ratio is roughly proportional to the rate of deformation energy generation as predicted by Eq. (2).

For the purpose of this study detailed calculations of temperature distribution as carried out by the previously mentioned investigations would be excessively time-consuming and not particularly enlightening. To control temperature rise in the material we must understand the effect of the following factors on peak temperature achieved in the extrusion process:

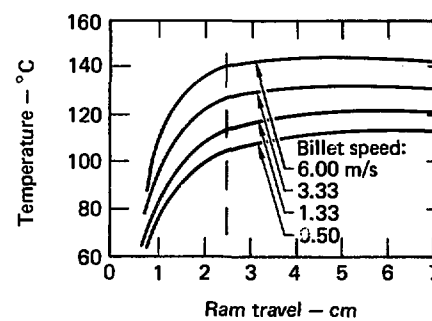

Fig. 19. Calculated curves of temperature rise of extruded material as function of extrusion progress (Ref. 18).

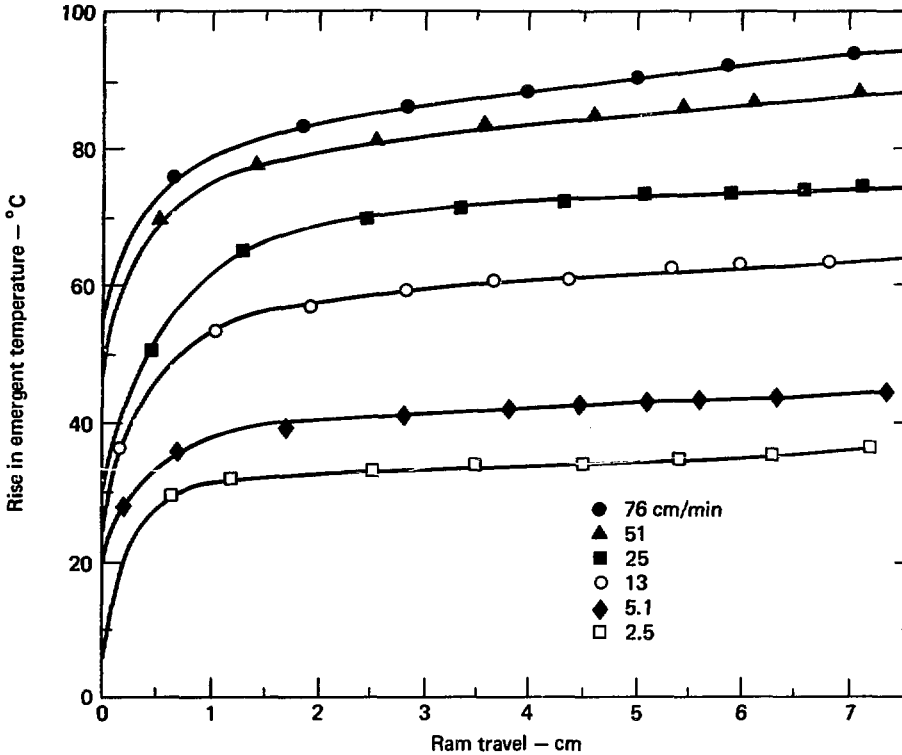

Fig. 20. Rise in emergent temperature as function of ram travel for Pb for reduction ratio of 29 (Ref. 19).

- Billet speed.
- Heat transferred from the extruded rod.
- Heat conduction from the deformation region.
- Reduction ratio.
- Billet diameter.
- All other factors determining the extrusion pressure.

For this purpose we have constructed a mathematical model that neglects the temperature variation over the cross section and deals only with the steady-state temperature. As shown in Figs. 18 through 21 these assumptions are well justified at sufficiently low speeds and low coefficient of friction. Figure 22 shows a schematic representation of the extrusion die and the position coordinates to which all of the formulation will refer. We will start by writing the steady-state heat balance for the billet and the extruded rod

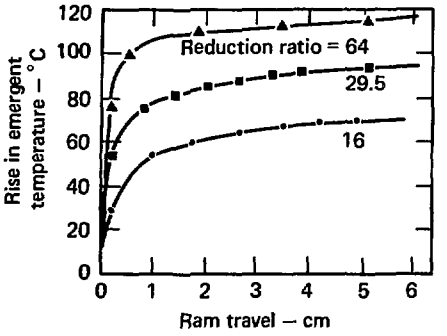

Fig. 21. Experimentally determined rise in emergent temperature as function of ram travel for Sn billets subjected to various reduction ratios (Ref. 19).

outside the deformation zone. In the billet we have

$$k \pi a_B^2 \frac{d^2T}{dx^2} - \pi v_B C a_B^2 \frac{dT}{dx} - 2 \pi a_B h_B T = 0, \quad (3)$$

where T is the temperature of the billet at position x along its length, k is the average thermal conductivity of the billet material, a_B is the radius of the billet, v_B is the speed of the billet, C is the heat capacity of the billet material, and h_B is the coefficient of surface heat transfer between the surface of the billet and the hydrostatic fluid medium.

A similar expression can be written for the extruded rod:

$$k \pi a_R^2 \frac{d^2T}{dx^2} - \pi v_R C a_R^2 \frac{dT}{dx} - 2 \pi a_R h_o T = 0, \quad (4)$$

where now h_o is the coefficient of surface heat transfer between the rod and whatever median surrounds it, a_R is the radius of the extruded rod, and v_R is the speed of the extruded rod.

In both of the above expressions we have assumed a uniform temperature distribution over the cross section of the billet or rod. The first term in the above expressions represents the process of heat conduction along the billet or rod; the second represents the transport of heat by the moving rod or billet; the last represents the heat transferred from the surface. In the deformation zone the heat-balance equation is more involved.

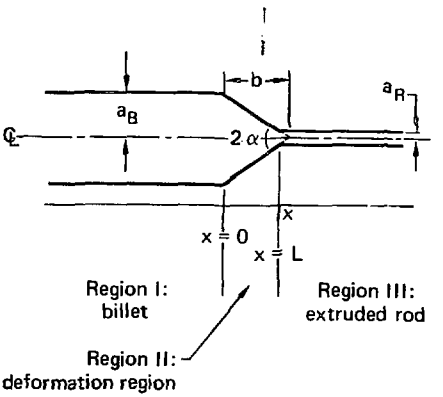

Fig. 22. Extrusion die, billet die, and position coordinates referred to by Eqs. (2) through (5).

Not only is the billet reducing in diameter as it passes through the die but also heat is being generated at a rate depending on the rate of deformation at any point in the deformation region. The differential equation within the die that occupies the length ℓ along the x axis is

$$k \pi (\tan \alpha)^2 (b-x)^2 \frac{d^2T}{dx^2} - v_B a_B^2 C \frac{dT}{dx} - 2 \pi h_o \tan \alpha (b-x) T + W(x) = 0, \quad (5)$$

where d is the die semi-cone angle, h_o is the surface heat-transfer coefficient between the billet and die surface, b is the constant equal to $a_B/\tan \alpha$, and W(x) is the deformation energy dissipated per unit length along the die.

To determine the steady-state temperature as a function of position, we must solve the differential Eqs. (3) through (5) and apply the boundary conditions, which are

$$T = 0 \text{ at } -\infty \text{ and } +\infty,$$

$$T_I = T_{II} \text{ at } x = 0,$$

$$\frac{dT_I}{dx} = \frac{dT_{II}}{dx} \text{ at } x = 0,$$

$$T_{II} = T_{III} \text{ at } x = \ell, \text{ and}$$

$$\frac{dT_{II}}{dx} = \frac{dT_{III}}{dx} \text{ at } x = \ell. \quad (6)$$

Analytic expressions for T_I and T_{III} are easily obtained for the corresponding homogeneous differential equations. However, an expression for T_{II} is considerably more difficult.

Sn-Cu Alloys and Their Reaction With Nb. In anticipation of our analysis and design of conductors including pure Sn or high-Sn-Cu alloys, we will discuss pertinent aspects of the diffusion and growth of phases in this system, the mechanical properties of the various alloys, and the composition dependence of the rate of Nb_3Sn formation.

The dependence of the rate of Nb_3Sn formation on matrix composition in solid-state reactions in bronze has been clearly established by Suenaga *et al.*[20] For up to 13-wt% Sn in Cu, the bronze matrix remains a homogeneous α phase throughout the processing of multifilamentary composites. Generally the rate of Nb_3Sn formation increases up to this concentration. As may be seen from the phase diagram in Fig. 23, concentrations of Sn exceeding 13.5 wt% at typical reaction temperatures between 700 and 800°C correspond to two-phased microstructures (including both the α phase and the δ phase[22]). These duplex structures are usually avoided in multifilimentary Nb/bronze composites because of their poor working properties and the possibility that

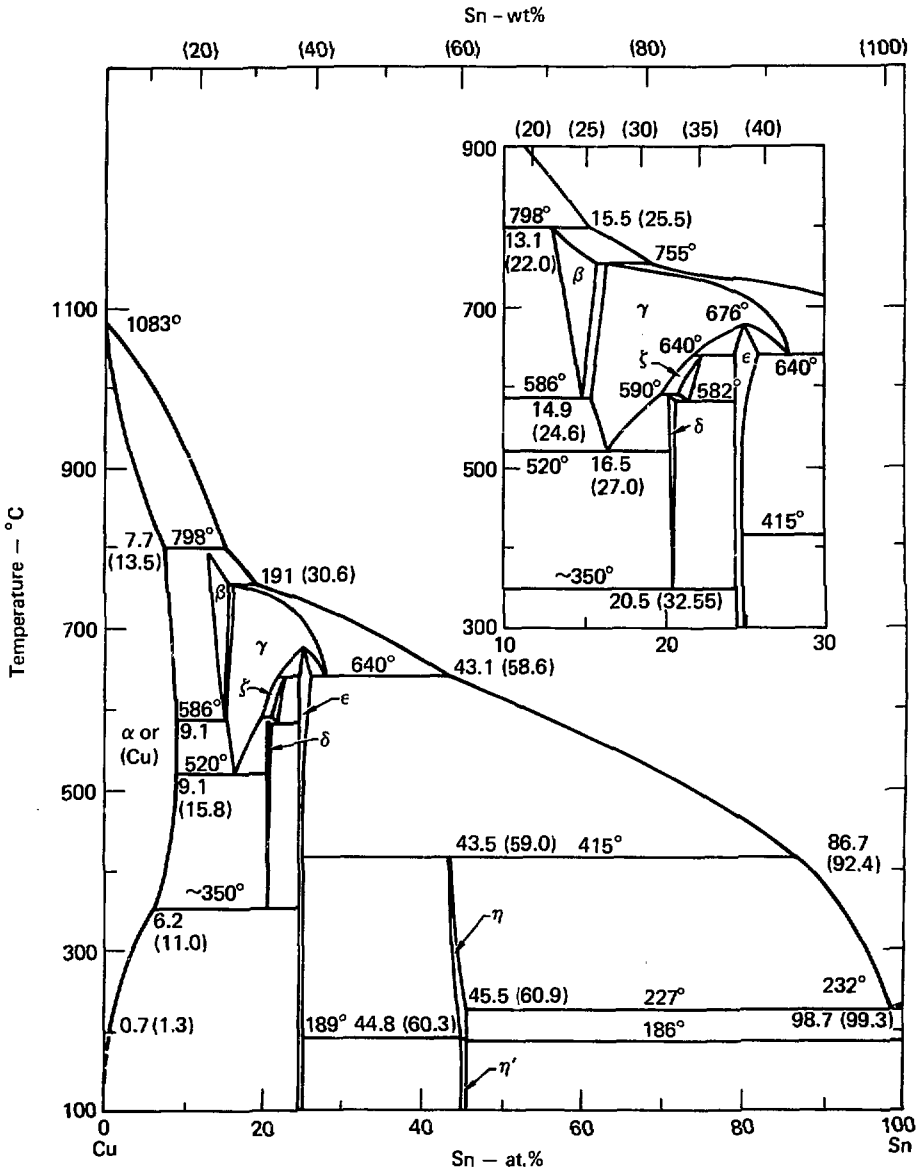

Fig. 23. Phase diagram for Sn-Cu system (Ref. 21).

the δ phase interferes with the growth of Nb_3Sn.[23]

Kinetic studies of Suenaga *et al.*[20] suggest that the rate of Nb_3Sn formation is severely reduced in the composition range corresponding to this two-phased structure. Whether this effect is the result of unfavorable kinetics of Sn diffusion to the Nb filaments in the formation of the A-15 phase or a thermodynamic effect involving the development of non-Nb_3Sn phases is not definitely known. However, investigations of Zwicker and Rinderer[23] clearly established that non-A-15 phases are formed when Nb reacts with Sn-Cu alloys having a higher Sn concentration than α-bronze.

There are several phases in the Sn-Cu system too brittle to be worked. For example, the ε phase, characterized by a narrow composition range of homogeneity around the stoichiometry Cu_3Sn, has been shown to be extremely brittle. This is probably true as well of the other phase of narrow compositional range, the η phase, which like the ε is stable at room temperature. Alloys in equilibrium at room temperature, which range in composition from 45-wt% Sn to 79-wt% Sn, are characterized by a two-phased structure of the η phase and a Sn solid solution saturated with Cu. These alloys are also characterized by a ductility roughly proportional to their Sn concentration. Although alloys of this compositional range are not as ductile as either pure Cu or pure Sn, composites including such alloys as shown by Hashimoto *et al.*[9] can readily be drawn through significant reductions without the need for intermediate anneals. This is probably a consequence of two fortunate qualities of these Sn-rich alloys: they are softer than the Cu matrix and the hydrostatic stress provided by the matrix is sufficient to prevent fracture of the alloy phase.

In view of the suspected adverse effects of non-α-bronze Sn-Cu phases on the growth of Nb_3Sn at the Nb filaments, we are taking the precaution in our proposed conductor designs of avoiding the growth of such phases among the Nb filaments. Consequently, the composite must be optimized with proper regard to two conflicting considerations. On the one hand we would like to eliminate as much of the Cu matrix as possible to increase current density; on the other hand enough Cu must be left as a buffer between the Sn alloy regions and the Nb filaments.

The work of Kawakatsu *et al.*[24] provides some important information regarding the growth of phases in a system consisting originally of pure Cu and pure Sn saturated with Cu. The phases appearing in diffusion couples generally include at least

some of the phases appearing in the equilibrium phase diagram at the given temperature. As expected, the study of Kawakatsu *et al.*[24] showed the orderly development of only the ε and η phases up to 410°C. Unexpectedly, however, the η phase still exists at 430°C when the phase diagram indicates a maximum temperature of 415°C for the η phase. The preferential growth of phases richer in Sn, such as η, is beneficial to the processing of the proposed conductor. The more concentrated the Sn alloy resulting from heat treatment, the more compact these non-α phases, which are detrimental to Nb_3Sn formation. An optimal homogenization heat treatment involves the greatest confinement of the non-α phases, which still permits the rapid diffusion of Sn through α-bronze.

The composite produced by Hashimoto *et al.*[9] involved pure Cu, Sn/20-wt% Cu and Nb in the ratios of 0.673, 0.151, and 0.176, respectively. After reducing the composite to about 0.127-mm diam without a single anneal, they heat treated the composite at 720°C for 50 h. Their photomicrograph of the composite following the heat treatment showed a cross section with no apparent void formation. However, for the small number of Nb filaments compared with commercial conductors now available, the composite produced by these authors was far from optimized.

Experimental and Analytical Investigations

This section describes the experimental and analytical studies performed to answer several important questions in the design of composites involving a reaction matrix of pure Cu and Sn-rich Sn-Cu alloy including

- The size and distribution of the Sn-rich elements. Sn must be distributed sufficiently to allow diffusion throughout the reacting matrix. The size of the Sn-alloy elements and their proximity to Nb filaments is restricted by the need to prevent growth of non-α-phase Sn-Cu alloy phases among the Nb filaments. The size of the Sn-alloy elements will also determine the distribution of Kirkendall voids. Present in all types of reacted multifilamentary composites, these voids should not be so large or so extensive that they interfere with the transport of Sn to the Nb filaments.
- The heat treatment that will minimize the spreading of non-α phases during the homogenization heat treatment prior to reaction. The more compact the Sn-rich regions after homogenization of Sn, the larger the Sn-rich elements may be.

- The procedure for producing elements for billet packing and billet extrusion. Conductor fabrication usually begins with an extrusion of a composite billet made up of hexagonal rods consisting of the conductor elements. The number of extrusion stages, the nature of the components at each stage of billet extrusion, and the extrusion reduction ratio are all important to the cost of conductor fabrication. They will therefore be considered in detail. The maximum extrusion ratio that may be accomplished by hydrostatic extrusion of billets containing high-Sn alloy will be studied through several experimental extrusions.
- Control of billet heating during operation. The minimum billet-extrusion cycle time will be determined by the likelihood of melting the Sn-rich alloy. In this study we observed the effects of temperature rise during the extrusion of a limited number of composite billets. By applying the formulation of the previous section, we will be able to extend our results to predict the heating effects at larger billet diameters and over greater ranges of speeds and reduction ratios.

Figures 24 and 25 show the cross section of the composite used in our diffusion studies at 0.38-mm diam and 0.20-mm diam, respectively. The composite consists of a core of Sn/16.7-wt% Cu in a pure Cu jacket.

Fig. 24. Experimental composite, used in diffusion studies, consisting of core of Sn/16.7-wt%-Cu within jacket of pure Cu. Composite diameter is 0.38 mm. Magnification: 300X.

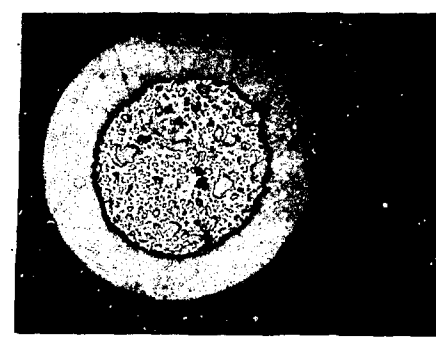

Fig. 25. Same experimental composite as shown in Fig. 24 but drawn to diameter of 0.20 mm. Magnification: 500X.

As can be seen from the figures, the core exhibits a duplex structure consisting of a matrix region of Cu-saturated Sn and particles of η phase as well as particles of η phase surrounding cores of ε phase. The existence of the ε phase is the result of coring during solidification of the alloy. The cast structure of the starting Sn alloy is shown in Fig. 26. There as well we see the duplex structure that exists as a dendritic structure with regions of Cu-rich phases consisting of cored regions having ε in the center and η on the outside. A feature worthy of note is the considerable degree of refinement of the particles of the Cu-rich phases as one draws the composite from its original diameter of 1.27 mm to the final diameter of 0.20 mm. This refinement of the brittle phase apparent from Figs. 24 and 26 represents an approximate average of reduction in cross-sectional area of the grains by a factor of 200.

Fig. 26. "As cast" structure of Sn/16.7-wt%-Cu alloy used to produce composite drawn in Figs. 24 and 25. Magnification: 200X.

In spite of the existence of the brittle phase the Sn/16.7-wt% Cu alloy in a pure Cu jacket may be drawn through significant levels of reduction without the appearance of drawing defects (e.g., chevroning, which is characterized by void regions near the center of an extrusion or drawn rod of a brittle material). The photomicrographs in Figs. 27 and 28 show sections along the length of the composite having the cross-section shown in Fig. 24. Not only is there no evidence of chevroning or other defects, there is no disturbance of composite uniformity by the more brittle phase.

In our design of a composite with a Sn-rich region in the reaction matrix, we have been more inclined toward a Sn-rich Sn-Cu alloy rather than pure Sn in the two-phased region of the equilibrium phase diagram. This preference is based on several considerations involving orderly interdiffusion during homogenization heat treatment and the integrity of the composite.

The work of Hashimoto *et al.*,[9] which involved a composite with such an alloy (Sn/20-wt% Cu), demonstrated the successful reduction of a composite with a two-phased Sn-alloy

Fig. 27. Longitudinal section of composite shown in Fig. 24. Magnification: 300X.

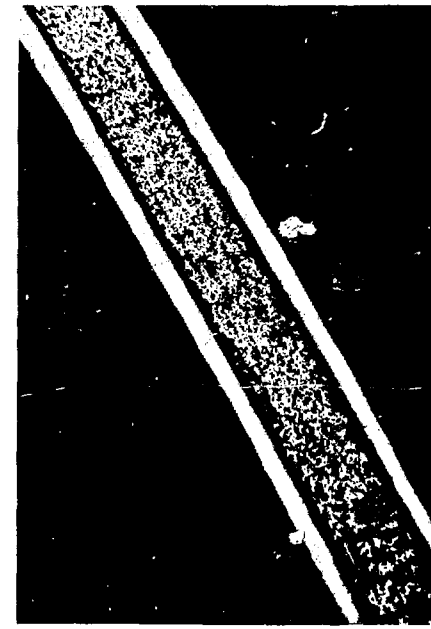

Fig. 28. Longitudinal section of composite shown in Fig. 24. Magnification: 90X.

constituent. The difference in hardness between pure Sn and pure Cu is large enough to lead to problems during extrusion of a composite with both constituents. To avoid distortion, which can occur when a softer constituent such as pure Sn is drawn in a harder material such as Cu, a small amount of Cu (up to 20 wt%) may be added to the Sn to increase the hardness of this constituent.

Another advantage of the Sn-Cu alloy over pure Sn is that the material can be contained more readily if melting occurs during hydrostatic extrusion. Rather than melting entirely at a single temperature, a Sn-rich alloy containing Cu will begin to melt at slightly below the melting temperature of pure Sn. It will, however, exist below the liquidus temperature as a partly molten material, with a distribution of a solid phase that impedes the flow of the molten portion of the alloy.

A third possible advantage of the Sn-Cu alloy over pure Sn is a more orderly interdiffusion resulting from

saturation of the Sn-solid solution phase with Cu. When the gradient in concentration is reduced between two components of a diffusion couple, generally the degree of Kirkendall-void formation near the original interface is considerably reduced. This is important to our composites because Kirkendall voids occurring near the original interface could conceivably interfere with diffusion of Sn throughout the composite.

The heat treatment of the proposed composite will have two stages. The first stage will allow the homogenization of Sn throughout the reacting matrix in preparation for the reaction to be carried out in the second stage of heat treatment. Since the reaction should not occur in the first stage, it must be carried out at a temperature below 600°C. An important consideration in the selection of the heat-treatment time and temperature is that at the chosen temperature, the Sn must exhibit a sufficient rate of diffusion in α-bronze. Also, the whole process must be completed with the greatest degree of confinement of non-α-phases. The optimal homogenization heat treatment may involve two or more stages. The initial experiments were only designed to delineate the important features of the diffusion process.

The composite used appears in Fig. 24. The overall diameter was 0.38 mm; the diameter of the Sn-rich regions was 0.234 mm. After a heat treatment of 400°C for 20 h, the composite cross-section had the configuration of phases shown in Fig. 29. The center region is the original two-phase mixture of Sn and η phase. The next ring of material going outward is pure η phase, followed by ε phase, and finally α phase. The pinkish color observed for the α phase indicated that at this temperature Sn had not diffused to an appreciable extent in the Cu. The data of Oikawa and Hosoi,[25] which indicate a diffusion distance [diffusion distance is defined as (diffusion coefficient x time)$^{1/2}$] for Sn in Cu of 4×10^{-5} cm after 20 h at 400°C, confirm the sluggish diffusion of Sn in Cu at this temperature. The heat treatment at 400°C was continued and the result is in Fig. 30. As this shows, after 68 h at 500°C, all of

Fig. 29. Cross section of composite wire after heat treatment for 20 h at 400°C. Magnification: 300X.

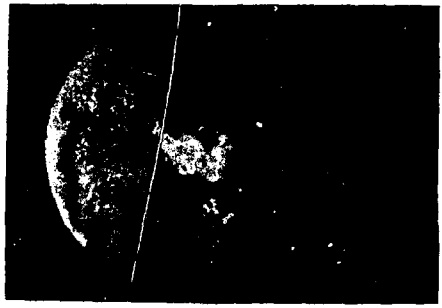

Fig. 30. Cross section of composite wire after heat treatment for 68 h at 400°C. Magnification: 300X.

the original Sn-rich phase mixture has been eliminated; the ε phase has grown; and the η phase, which now occupies the center, has reduced. The outer region of almost pure Cu still does not show any appreciable extent of Sn diffusion into the Cu. If the heat treatment at 400°C were allowed to continue, all the η would probably be converted to ε phase before even a small fraction of the Sn could diffuse into the Cu.

Figure 31 shows a sample of the composite in Fig. 24 after a heat treatment of 68 h at 600°C. Two phases are apparent in this photomicrograph. The phase near the outside is a bronze through which an appreciable amount of Sn has diffused. The central region with the specked appearance consists of the ε phase and small regions of α-bronze. This phase mixture results from the decomposition of the δ phase, formed at the heat-treatment temperature (600°C). Judging from the quantities of the two phases shown in this section, the composite must be close to equilibrium.

The distribution of the ε phase shown in this photomicrograph is quite irregular. Most likely this is a consequence of growth of the non-α-phases and subsequent decomposition of such phases (as diffusion of Sn into the Cu is allowed to proceed). The circle fully containing the remaining ε phases is the region in which no Nb filaments should exist in a superconducting composite that has all three constituents.

For the sake of selecting a heat treatment that will result in the greatest confinement of the ε phase, a comparison of the extent of ε phase resulting from the two heat-treatment temperatures will be useful. From the photomicrograph of Fig. 30 we may calculate the ratio of the diameter of

Fig. 31. Sample of composite shown in Fig. 24 after heat treatment for 61 h at 600°C. Magnification: 300X.

the circle fully circumscribing the non-α-phase region, d_f, to the diameter of the original Sn-alloy filament, d_i:

$$d_f/d_i = 1.46 \qquad (7)$$

(after a heat treatment of 68 h at 400°C). At this point in time during the interdiffusion of Sn and Cu, the η phase has not been completely converted to ε phase. The final extent of the ε phase is thus expected to be worse that that indicated by Eq. (7).

A similar ratio may be established for the heat treatment carried out at 600°C as represented by the photomicrograph of Fig. 31:

$$d_f/d_i = 1.340 \qquad (8)$$

(after a heat treatment of 61 h at 600°C). The results would tend to recommend the 600°C heat treatment over a lower temperature heat treatment (such as one at 400°C) for homogenizing the composite prior to reaction. The advantage of a higher temperature probably results from a high rate of diffusion of Sn in Cu occurring simultaneously with the growth of the other phases. A homogenization carried out at a temperature greater than 600°C may result in even greater confinement of the ε or δ phase. It would, however, present the danger of premature reaction and consequently a poor distribution of Nb_3Sn over the groups of Nb filaments.

Although homogenization heat treatment is subject to further optimization, these preliminary results will be used for the design of our composites. With 600°C as the acceptable homogenization temperature we will use the relationship of Eq. (8) as an indication of the region from which Nb filaments must be excluded. Kirkendall voids are always present after reaction of a multifilamentary Nb_3Sn composite. However, bronze/Nb composites, externally tinned Cu/Nb composites, and Cu/Nb/Sn alloy composites differ in the nature and distribution of these voids.

In bronze/Nb composites voids generally become distributed throughout the Nb filaments. In externally tinned or Cu/Nb/Sn composites Kirkendall void formation is usually restricted to the interface between α regions and the δ phase that forms early in the interdiffusion process. In the composite of Fig. 31 these voids exist on or somewhat outside the circle of diameter d_f. If, in the design of a composite, we distribute the Nb filaments up to the circle of diameter d_f, we permit only an insignificant fraction of the filaments to be affected by voids. The percentage of Nb filaments affected by voids in such a composite will undoubtedly be less than that in

a typical bronze/Nb composite after reaction.

Kirkendall voids must not be extensive enough to interfere with the diffusion of Sn throughout the composite. The observation of many sections of the composite of Fig. 31 revealed no void regions so extensive. Figure 32 shows photomicrographs of several other sections of this heat-treated composite. Under direct observation the outer α-bronze regions always appeared uniformly yellow.

The construction of billets in the production of large quantities of superconducting composites generally involves the stacking of hexagonal elements into a hollow cylindrical can. In preparing billets used in the hydrostatic extrusion experiments we used such a stacking method. We prepared hexagonal elements consisting of cores of pure Sn and Sn/16.7-wt% Cu alloy. Both of these elements had cores occupying 70% of their cross-sectional area (Figs. 33 and 34). Groups of seven hexagonal elements were stacked into the billet shell as shown in the schematic representation of the billet cross-section in Fig. 35. The dimensions of the composite billet are in Figs. 35 and 36. The tail cap and nose of the billet were secured to the body of the billet by electron-beam welding. Photographs of these welds appear in Figs. 37 and 38.

Fig. 32. A 0.38-mm-diam Cu/Sn-16.7-wt%-Sn composite interdiffused for 60 h at 600°C. Views (a) through (c) show representative cross sections photographed at different positions along wire.

A feature worthy of mentioning is the very successful drawing of a composite containing pure Sn and Cu. This may suggest that the precaution

Fig. 33. Cross section of hexagonal elements used in packing billets used in study of hydrostatic extrusion. This hexagonal rod is 0.450 cm side to side. The core, which is a Sn/16.7-wt%-Cu alloy, occupies 70% of cross section.

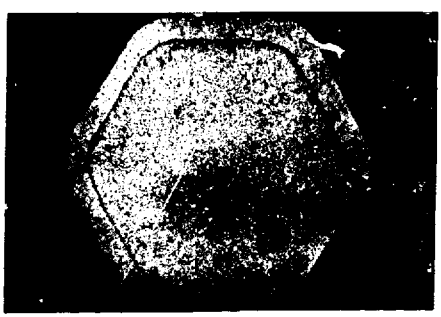

Fig. 34. Cross section of hexagonal element having as its core pure Sn. This hexagonal rod is 0.450 cm side to side. The core occupies 70% of composite.

of alloying the Sn with Cu to increase its hardness is not necessary. If this is generally true there would be much greater freedom in designing composites and probably a reduction in conductor cost.

The important consideration with regard to these composite billets is the maximum reduction ratio permissible before some disruptive effect such as the melting of the Sn alloy occurs. The work of extrusion converts almost entirely to heat, which is partly dissipated and which partly contributes to billet heating. For Sn to melt, enough of the mechanical energy of extrusion must be absorbed by the billet to raise its temperature above the melting point of Sn. The Sn alloy also must have time to absorb the latent heat of fusion. With all these factors involved we cannot immediately accept the adiabatic temperature calculated from the extrusion pressure as an indication of the temperature achieved by the billet. We also cannot assure that merely reaching the melting point

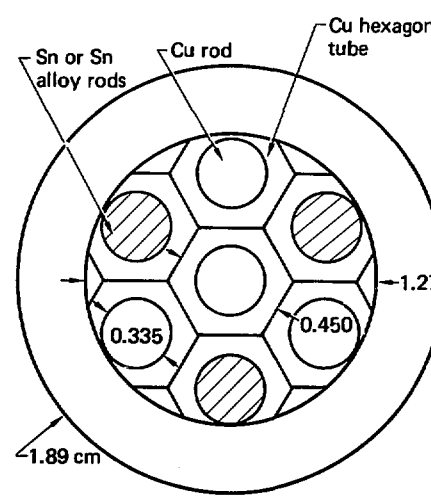

Fig. 35. Cross section of billet showing stacking of elements.

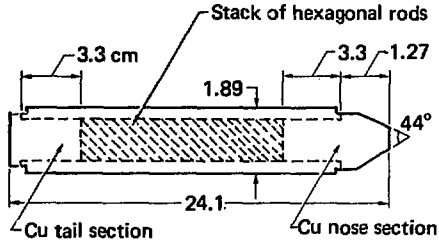

Fig. 36. Billet used in hydrostatic-extrusion experiments.

results in billet disruption. Most likely the billet temperature must exceed the melting point with a sufficient margin so the latent heat is accepted by the Sn during the deformation of the composite.

A superconducting billet containing Nb, Ta, soft Cu, and the Sn alloy will most likely have a flow stress

Fig. 37. Weld at tail section of experimental billet.

Fig. 38. Weld at nose section of experimental billet.

between hard and soft Cu. To provide a difference in component hardness not less than that existing in an actual composite billet, IGC used hard Cu rather than soft Cu in the experimental extrusions. The choice of hard Cu also guaranteed that the calculated adiabatic temperature rise would exceed the melting point of the Sn alloy for the extrusion ratios available to us. The purpose of these preliminary extrusions was to establish the possibility of producing a round extrusion in a composite billet containing the Sn alloy and to gain a rough idea of the limitations on permissible extrusion ratio.

Because of the presence of the low-melting-point Sn alloy, extrusion must be carried out with billets at room temperature or below. Because of the extremely high pressures associated with cold conventional extrusion of Cu and the other composite constituents, hydrostatic extrusion is absolutely essential.

The extrusion should reduce the billet to a diameter less than 12.7 cm, which is the limit of presently practical draw-bench drawing. The higher the reduction ratio of the extrusion, the more economical the process (since higher extrusion ratios eliminate more of the draw-bench drawing that must be carried out in successive passes with limited reductions per pass).

Of the three extrusion ratios attempted only two (4.7- and 9.5- to-1 reduction in area) could be accomplished because of the limitation in pressure (1600 MPa). The extrusions were interrupted when about 4 cm of the billet remained. This allowed us to examine the region remaining in the die. Figure 39, which shows the billet extruded at 4.7-to-1 reduction in area, reveals some chatter as a result of uneven and inadequate lubrication. The 9.5-to-1 reduction in area on the other hand revealed a smooth surface at the die interface (Fig. 40). Apparently at the higher pressures needed to carry out the higher reduction ratios, lubrication of the die/billet interface by the extrusion fluid is more effective. The cross-section of the billet extruded at 4.7-to-1 reduction ratio showed regions of nonbonding (as did the rod extruded at 9.5-to-1). Cross-sections of the two rods are in Figs. 41 and 42, respectively. The 9.5-to-1 reduction resulted in melting and rupture of the billet. Table 4 summarizes the results of the hydrostatic extrusions.

The graph in Fig. 43 provides the extrusion pressures corresponding to the extrusion ratios of our composite billets along with estimates of pressure for the extrusion of soft Cu. The corresponding adiabatic temperature rises are likewise indicated on

Table 4. Summary of hydrostatic-extrusion experiments.

Reduction in area attempted	Extrusion pressure (MPa)	Peak pressure at beginning of extrusion (MPa)	Billet speed (m/min)	Estimated adiabatic temperature rise[a] (°C)
4.7 to 1	690	no peak	1.8	200
9.5 to 1 (melting)	1055	1380	1.8	305
9.5 to 1 (melting)	1000	1380	0.9	290
16 to 1	Initial peak pressure prevented this reduction			

[a]The temperature when no heat conduction occurs along the billet or rod or to the tooling. It will be the peak temperature experienced by the material in the limit of high extrusion speeds.

Fig. 39. Region remaining in die after interruption of 4.7-to-1 extrusion [1.8-m/min billet velocity].

the ordinate of this graph. The 4.7-to-1 reduction falls below the pressure corresponding to the melting temperature of Sn. The 9.5-to-1 reduction, however, is significantly above this pressure.

In the extrusion of a superconducting composite we can be sure of accomplishing at least a 4.7-to-1 reduction ratio. This would correspond to a 25-cm diam billet extruded to a 11.7-cm diam rod that can be readily handled by existing draw benches.

An alternative to accepting the 4.7-to-1 reduction ratio and continuing the reduction with bench drawing is carrying out the extrusion

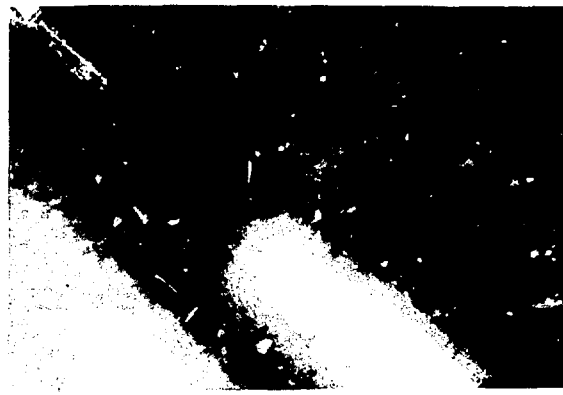

Fig. 40. Region remaining in die after interruption of 9.5-to-1 extrusion [0.9-m/min billet velocity].

Fig. 41. Cross section of rod extruded with 4.7-to-1 reduction ratio and billet speed of 1.8 m/min.

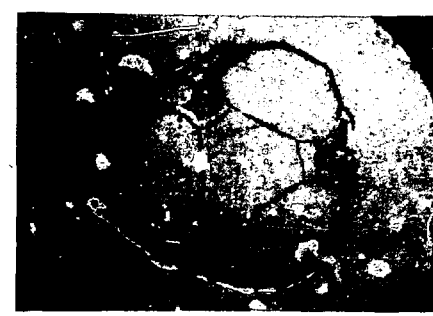

Fig. 42. Cross section of rod extruded with 9.5-to-1 reduction ratio and billet speed of 1.8 m/min.

at a higher ratio with cooling of the extruded rod. The crucial consideration in evaluating the possible economic advantage of the latter alternative is the extrusion speed required to allow sufficient heat conduction from the deformation zone through the extruded rod to the cooling medium. Using the previously developed formulation with several simplifying but conservative assumptions we arrive at the following expression for the maximum temperature achieved by the extruded billet:

$$T_{max} = \frac{\rho}{2C}\left[1 + \left(1 + \frac{8hk}{C^2 v_R^2 a_R}\right)^{1/2}\right], \quad (9)$$

where C is the heat capacity of the billet material, v_R is the velocity

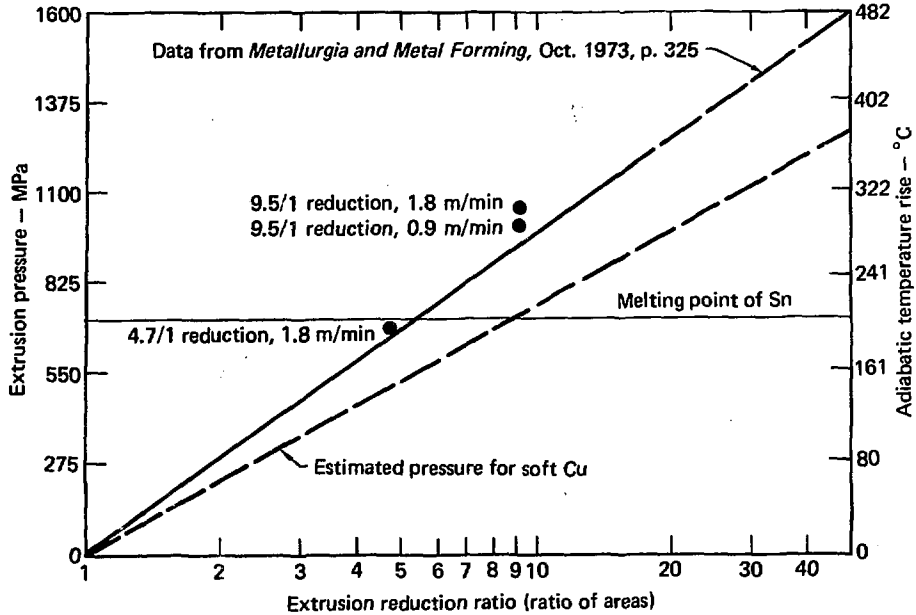

Fig. 43. Extrusion data for two experimental billets compared with behavior anticipated for soft Cu.

of the extruded rod, a_R is the radius of the extruded rod, k is the thermal conductivity of the composite material, and h is the surface heat-transfer coefficient to the cooling medium.

Using values for pure Cu we have calculated the temperature rise corresponding to the extrusion of a billet at a speed of 0.04 m/min for a range of extrusion ratios. The extrusion pressure as a function of area reduction ratio used in the calculation corresponds to the trend followed by our composites consisting of hard Cu and Sn/16.7-wt% Cu elements. The value of h was determined from the data for boiling water heat transfer of McAdams[26] along with the assumption that the heat originates from a surface at half the radius of the extruded rod.

Figure 44 has the results of these calculations along with the data from the extrusion of our experimental composites.

Economic Considerations

To assess the economics of the high-Sn process relative to conventional α-bronze processing we developed four conductor designs. Each was designed to carry 10 kA at 12 T

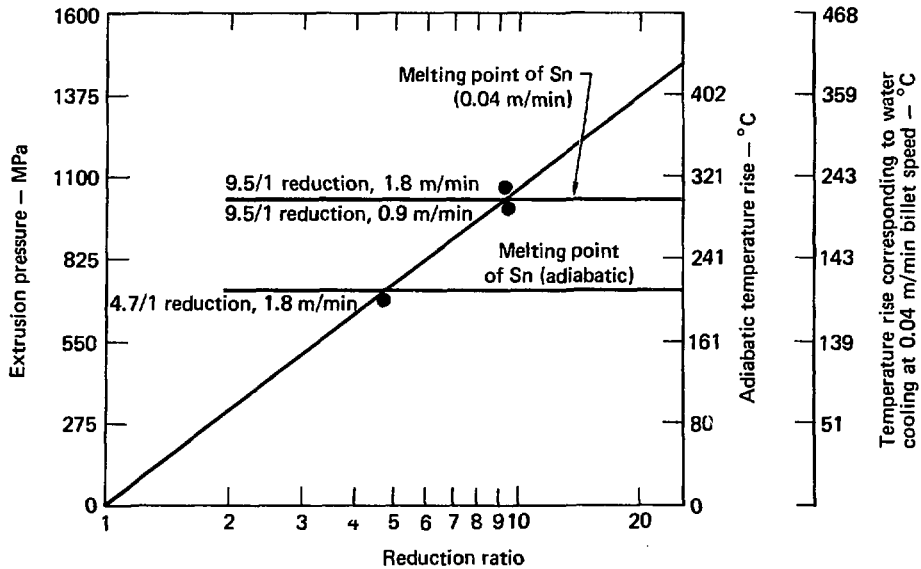

Fig. 44. Temperature rise as function of reduction ratio for composite billet extruded at speed of 0.04 m/min with water-cooling of exiting rod.

and each employed Ta-protected Cu regions. We considered solid and hollow filaments. The economic factors were

- The amount of reactive matrix necessary to form the required quantity of Nb_3Sn.
- The J_c of the Nb_3Sn formed (dependent on Sn concentration)
- The cost of the individual processing steps.
- The yield per extrusion.

The results indicated that the cost per pound of conductor was virtually identical for both types of material, but that the high-Sn bronze required less weight of conductor for the same current due to a higher overall J_c. This gave it a net advantage of about 40% in cost per ampere metre.

Ongoing Work

At present further work on this program has not been funded.

High-Field Cryogenic Tensile-Test Experiment

One of the more interesting, and controversial, aspects of multifilament Nb_3Sn conductors is their mechanical properties. Because of the inherently brittle nature of Nb_3Sn it can contribute to at least two potential problems. First, as

the volume fraction of Nb_3Sn is increased to achieve higher overall J_c's a critical point is reached where the entire conductor will exhibit a low strain-to-failure in a conventional uniaxial tension test. This effect, not unique to Nb_3Sn conductors, is a general feature of a ductile matrix reinforced with brittle fibers as discussed by Old and Charlesworth.[8] Conductors now being processed are apparently approaching, or exceeding, this critical volume fraction as discussed earlier in "LLL/Airco Program Results." This fact does not in any way indicate that such Nb_3Sn conductors are unusuable, merely that the mechanical properties of the composite as a function of composition and geometry must be considered as one of the variables in the overall conductor and magnet design.

The second potential problem is the fact, observed experimentally, that tensile stress can reduce the current-carrying capacity of Nb_3Sn. In general the reduction becomes observable for strains > ~0.2% and becomes progressively larger for increasing strain levels. For a given strain level the amount of reduction is field dependent, increasing for higher field levels. At the present time insufficient data exist to sufficiently integrate this effect into conductor designs in a quantitative manner.

Because of the importance of these effects on conductor design and optimization we decided in late FY75 to create testing equipment to obtain the relevant data on the prototype conductors being developed under contract in industry. Since a variety of materials would need to be tested we designed the equipment to be as versatile as possible while maintaining reasonable ease of operation.

The basic idea of our system is to be able to measure the critical current of specimens in fields up to 12 T while simultaneously applying a uniaxial strain to the specimen. In this manner one can reasonably approximate actual operating conditions of a conductor in a coil. Assembly of this equipment began in FY76.

The hydraulic power console and the load-frame structure appear in Fig. 45. We chose a hydraulic-powered piston, as compared with a screw-driven crosshead, since either load or strain control could be used. The load frame, constructed of stainless steel to avoid any interaction with the magnetic field, will operate up to a maximum applied force of 2.2×10^5 N. The crosshead, raised

Fig. 45. Load-frame structure and hydraulic controls for tensile tester.

and lowered by hydraulic pistons, can be hydraulically clamped on the guide columns at any desired position.

After assembly, we used the system at room temperature to verify proper operation and to determine the room temperature and mechanical properties of the conductors to be subsequently studied at 4.2 K. For this mode of operation the lower grip attaches to the lower support beam (Fig. 46).

Figure 47 exemplifies the type of stress-strain data obtained at room temperature for an Airco 1-kA conductor using 10-wt%-Sn bronze. Table 1 provides the details of this material. We measured the strain using a conventional foil-strain gage and recorded the data on magnetic tape using a small computer-data acquisition system. The failure point in this figure at 0.95×10^5 μm/m is the point where the strain gage failed. (The sample failed at 1.6×10^5 μm/m as determined by gage marks on the sample.)

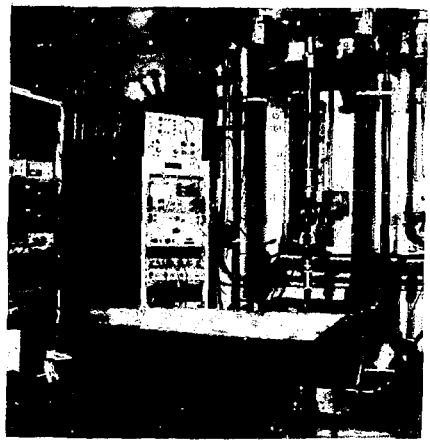

Fig. 46. Tensile tester set up for room-temperature measurements.

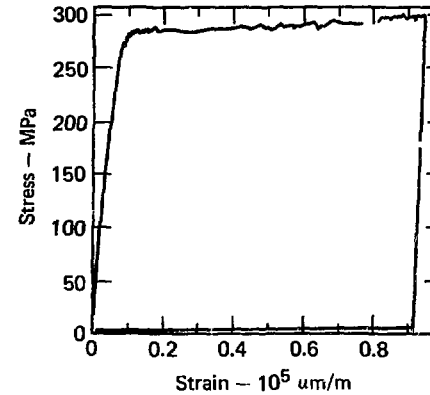

Fig. 47. Room-temperature stress-strain data for Airco 1-kA, 10-wt%-Sn bronze conductor.

For cryogenic measurements, the mechanical load is returned to the crosshead by a compression structure using three cylindrical columns. This structure was designed for a maximum force of 90 000 N because this should be sufficient for all the early measurements to be performed. Figure 48 shows this structure being lowered into the cryostat. The upper grip, constructed from 21-6-9 steel, is visible above the edge of the cryostat. The complete assembled system is in Fig. 49. The height of the vertical columns (5.3 m) is such that the cryogenic structure can be raised and the cryostat rolled out from underneath to change samples.

The system will be operated at 4.2 K early in FY77, then the magnet will be installed for the initial strain-effect

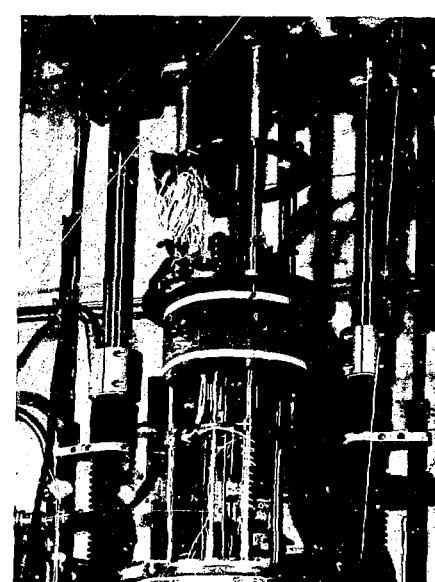

Fig. 48. Cryogenic structure, with top stainless steel wedge grip being lowered into cryostat.

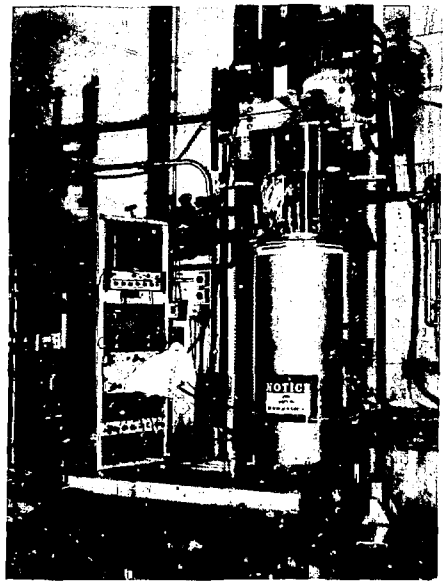

Fig. 49. Cryogenic tensile tester completely assembled for 4.2-K mechanical measurements.

measurements. This magnet is the same one we have previously used for short-sample measurements.

In parallel with the construction and testing of the tensile tester we have been evaluating commercial metal-foil strain gages for use in instrumenting samples to be tested as well as for use in future magnet systems such as MFTF. Testing and evaluation is proceeding as follows:

- Evaluate apparent-strain characteristics of different compensation gages on various appropriate substrates.
- Measure change in gage factor between room temperature and 4.2 K.
- Determine acceptable power-dissipation levels for different thermal environments.
- Determine magnetic-field effects.

Before initiating this work we held several conversations with P. Wahlstrom of the Oak Ridge National Laboratory and J. Ekin of the National Bureau of Standards (Boulder) about the use of strain gages at low temperatures and in high magnetic fields. Their work, and previous work at LLL on the Baseball coil-structure instrumentation, led us to conclude that the Micro Measurements Karma alloy was the most appropriate to investigate. Previous work also showed that the WK series gages produced by Micro Measurements using this alloy were the best for our use.

Starting at this point our first experiment was to determine the most appropriate compensation for use on various materials at 4.2 K. Compensation refers to the strain-gage expansion coefficient at room temperature with standard values being 6, 9, 13, and 15 ppm/°F. We mounted WK gages of each compensation on one side each of 316 stainless steel, 21-6-9 stainless steel, OFHC Cu, a 3.5-kA Airco conductor, and a Nb-Ti

composite conductor. Four of these samples ready for use appear in Fig. 50. On the back of each sample we mounted a Micro Measurements CLTS temperature sensor. The samples were hung off a rod at the top of a liquid-helium (He) cryostat with a small amount of He in the bottom. By slowly lowering the samples down into the cryostat and taking data at the rate of 10 points/s, we could obtain a temperature-dependent apparent-strain curve for all the gages in a single run. Data was taken both warming and cooling. Figure 51 shows a computer-generated plot of the data for the OFHC Cu sample. For all five materials the 15-compensation gage gave the lowest offset at 4.2 K. Thus all our subsequent evaluations were on this type of gage.

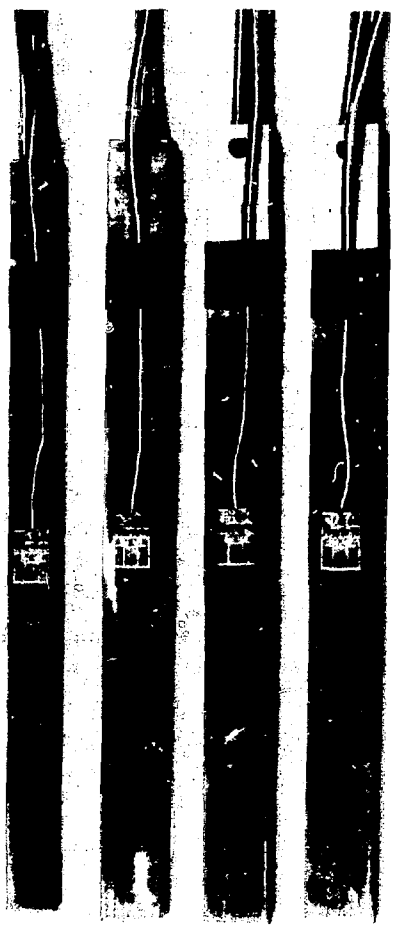

Fig. 50. Four apparent-strain test samples ready for use. The temperature sensors are mounted on backs of samples.

One added important point in Fig. 51 is the steep slope of the apparent-strain temperature curve near 4.2 K. This shows that self-heating effects due to excessive power dissipation or improper cooling can cause relatively large errors.

The system used to measure the temperature dependence of the gage

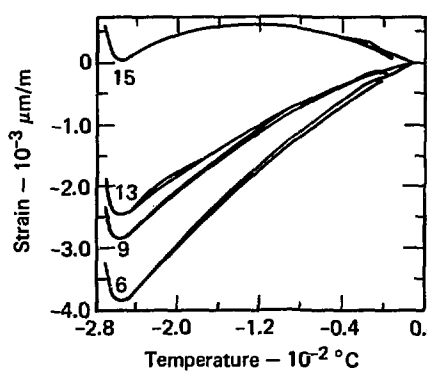

Fig. 51. Apparent strain as function of temperature for 15-, 13-, 9-, and 6-compensation WK gages on OFHC Cu.

factor, k, was constructed in a manner similar to that described by Telinde.[27] An Al flexure (with the gages mounted on it) is strained to a given value in bending by various-diameter supports and then temperature-cycled. Since strain remains constant at all temperatures the gage factor can be computed from the temperature-dependent output voltage. It is necessary to compensate for apparent-strain effects, which can be done by first determining this quantity in a run with zero-applied strain. The calibration fixture is disassembled in Fig. 52 and assembled in Fig. 53. The aluminum flexure and the side supports are all cut from the same 2024-T3 Al plate with the same orientation to minimize differential contraction effects. We made tests with this fixture on gages in both tension and compression at applied strains of 500 and 1100 με. The change in k between room temperature and 4.2 K was +4% ± 0.5% in all cases.

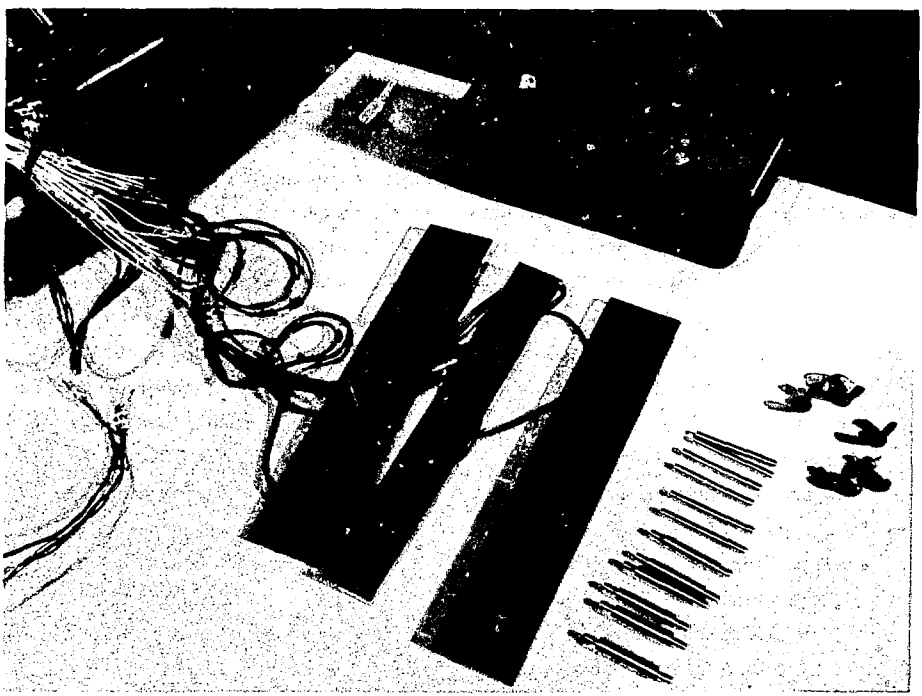

Fig. 52. Gage-factor calibration fixture ready for assembly. The various diameter pins shown allow strains up to 2000 μm/m to be applied to the flexure.

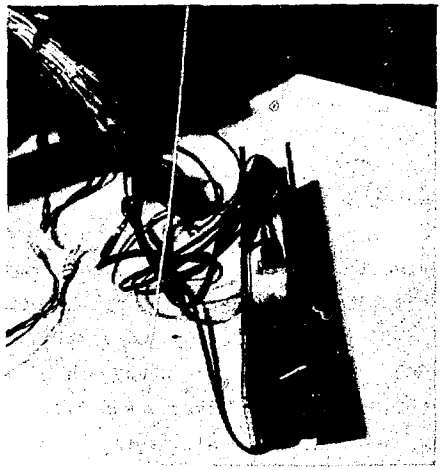

Fig. 53. Completely assembled gage-factor calibration fixture.

The power dissipation-thermal environment and magnetic-field effect measurements will be made in FY77. We intend to purchase a large quantity (several hundred) of identical gages once we have determined what their specifications should be. When we have these gages a number of them will be selected at random and run through all the calibration and evaluation measurements. These data will then be a basis for using the remainder of the gages in actual conductor or magnet diagnostics.

MAGNET DEVELOPMENT FOR MFTF

A development program has now been established to support the preliminary design concept of the superconducting yin-yang coils proposed in FY75 for the MFTF mirror machine. More detailed stress-analysis calculations carried out both at LLL and in industry confirm that stresses induced by the large magnetic forces can be limited to acceptable values by essentially using the case of one coil to act as a "C" clamp for the other coil. This analysis continues with more refinement to optimize both the structure and neutral-beam access and to ensure that stresses at joints and discontinuities are not excessive. The strength of the winding is ignored in these calculations, and the cumulative force on the conductors is assumed to be directly transmitted to the coil case. A stress analysis of the winding will follow when the strain of the coil case has been determined.

The Nb-Ti superconductor will be cryostatically stabilized in "pool"-boiling liquid He at 101 325 Pa (1 atm). Heat-transfer characteristics from a surface to liquid He highly depend on surface conditions and orientation. A conductor is thus being developed with a cooling surface added inside the conductor in such a way as to reduce the sensitivity of its heat-transfer coefficient to orientation. Our previous annual

report[5] indicated one possible conductor configuration in which four Cu conductors, one of which contained all the superconducting filaments, are soldered together to give a 12 × 12 mm conductor (Fig. 54). This arrangement and the alternative in Fig. 55 are now being developed in industry. Cooling channels and He-access holes are rolled and punched into a strip of stabilizing Cu in this alternative fabrication method. Again, all the superconducting filaments are contained inside a square conductor (about 6 × 6 mm) on which is electroplated a thin layer of 90Pb-10Sn solder. A continuous production line will be set up to wrap the stabilizing strip around the central core, melt the solder in a heating zone, and quench it with the conductor under pressure on all four sides.

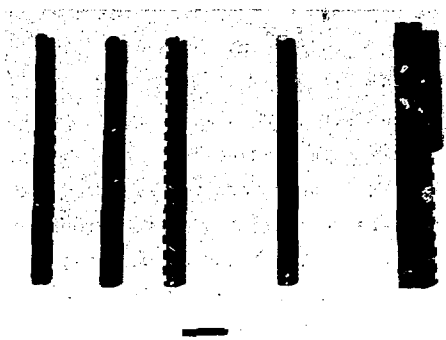

Fig. 54. "Four Bar" stabilized MFTF prototype conductor.

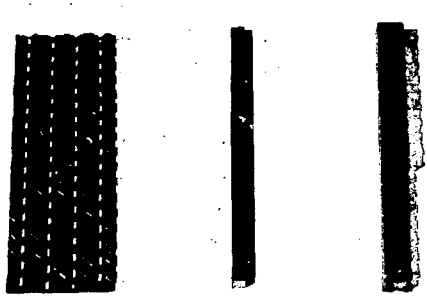

Fig. 55. "Wrap-Around" stabilized MFTF prototype conductor.

We ordered a billet of superconducting core from each of four major superconductor manufacturers in the U.S.A. This should yield about 2100 m of conductor. We plan to stabilize this material, using one of the alternative fabrication techniques, then build a 1-m-bore test coil with the finished conductor. While tests on short samples of the superconducting core are adequate to determine its superconducting properties, such tests cannot be used to investigate the effectiveness of the stabilizer. The purpose of the test coil is to check this property and, from the results, determine the operating current and safety margin. The maximum field at the conductor of this test coil will be boosted to ~6.5 T by mounting it between the first two "backing" coils for HFTF. Extrapolating the performance at 6.5 T to that at 7.5 T is not difficult.

We are still investigating a method for joining the conductor. While the explosive technique previously described[5] makes an excellent joint, it would be difficult to use this method to make the joints between pancakes, particularly the outside joints. A large containment vessel is necessary for safety reasons; also this prevents the joint from being made close to the winding. The alternatives under consideration include solder, cold welding, and diffusion bonding.

HIGH-FIELD TEST FACILITY

An integral part of the LLL Nb_3Sn development program is the testing of prototype conductors (1, 3.5, and 10 kA) in actual coils at each of the major development steps. Results on a coil wound from 1-kA conductor and tested to 10 T were discussed earlier in "LLL/Airco Program Results." To test conductors of about 3.5 kA in coil form, LLL, in early FY76, proposed to construct HFTF. The facility was subsequently approved for construction.

As discussed previously[28] HFTF involves a set of four Nb-Ti coils that, when stacked axially, form a solenoid 1.1-m long with a 1-m-clear bore and 1.8-m o.d. capable of generating a peak field of 8 T. A set of three Nb_3Sn coils will be stacked axially within this solenoid to generate a peak field of 12 T in a 0.4-m bore. A composite Nb-Ti/Nb_3Sn system is used to achieve a minimum materials cost for the 12-T peak field. Three, rather than one, Nb_3Sn coils are used so that only the innermost coil need be replaced to test a new material and to minimize the cost of a coil failure.

The coils are all designed to operate cryostatically in pool-boiling He. The conductors are aspected and will be wound flat with face-cooling channels. The Nb_3Sn conductors, similar to those listed in Table 1, will be stabilized by a Cu strip with integral cooling channels soldered onto the wide face.

At the present time the HFTF cryostat (2.1-m diam × 3-m length) has been released for fabrication and delivery in early FY77. An Nb-Ti conductor for two of the four coils is being obtained from the Princeton Plasma Physics Laboratory. The cryostat and these two coils will be used to test the MFTF test coil discussed in the previous section. This test is scheduled for late FY77. Plans have been made for moving the Airco 100-litres/h liquefier and

associated 10 000-litre storage Dewar, previously used on the Baseball II-T experiment, into the cryogenics laboratory as part of HFTF. This move is scheduled for late February 1977.

The next step in the construction of HFTF will be to acquire the Nb-Ti conductor for the two remaining backing coils and then to begin purchasing an Nb_3Sn conductor. This work will proceed as funds become available.

SUMMARY

During FY76 this group's work had two main goals:

- Development of multifilamentary Nb_3Sn superconductors for large fusion devices.
- Development of a conductor for MFTF.

The Nb_3Sn development work is a continuation of the program initiated in FY74 to develop a superconductor for large fusion systems. This superconductor will have a nominal rating of 10 kA at 12 T and a current density of 10^4 A/cm^2. Fabrication development continued at both Supercon and Airco using the Nb-tube and rod/bronze techniques, respectively. We refined the methods of measuring the properties of these development conductors to increase their sensitivity. Previous tests had shown the conductors to be capable of carrying high currents before going "normal"; but increased sensitivity was required to detect the onset of resistance. We had to know this onset because the limiting current in a large coil may be determined by resistive losses rather than by the "quench" current.

Data on both types of conductors were obtained at resistivities of 10^{-11} Ω-cm, compared with ~10^{-10} Ω-cm at the quench current. This data indicated that a current density of 10^4 A/cm^2, and in some cases as high as 3×10^4 A/cm^2 (excluding the space occupied by Cu), could be achieved in the conductors at this level of detection. Higher resolution could not be obtained from measurements on short samples because the signals were swamped by the voltage required to drive current across the bronze matrix from the outermost filaments to the inner ones as the conductor entered the high-field test region. In the low-field region the current could be carried in the outer filaments only; in the high-field region all the filaments carried current. The length of conductor in the field must thus be longer than is possible in the short-sample test equipment. Improvements in the power supplies

for the 27-cm-bore Nb_3Sn coil and Nb-Ti backing coil enabled higher resolution to be obtained on the Nb_3Sn than was reported in FY75. By measuring across two turns in the high-field region one can detect a resistivity of less than 10^{-12} Ω-cm.

Scaling up the small Airco experimental billets to 20-cm diam accentuated difficulties with the Ta barriers. Means of overcoming this are now being pursued. Room-temperature tests on our recently commissioned tensile tester also revealed that conductors processed identically may have widely varying ductility properties. Other workers saw this, and the popular explanation is that there is a critical ratio of Nb_3Sn (and perhaps Nb) to matrix cross-sectional area that, if exceeded, causes the whole conductor to fracture as the first few filaments break at a strain of ~1%. This hypothesis is being explored to ensure that future conductors behave overall as ductile materials.

The testing and proving of these new conductors in production lengths must continue to be demonstrated by building and operating full-scale coils. A new set of Nb-Ti backing coils, 1-m bore, complete with its cryogenics, is thus being built to house and test larger conductors and coils. The fabrication of the cryostat for this facility (HFTF) is due for completion by the end of December 1976. We will start on the coils during FY77.

Intermagnetics General studied a new processing technique using Sn-rich bronzes. This work concluded that possible savings of 40% in conductor cost may be achievable. Unfortunately, to obtain this benefit, a significant amount of development work needs to be performed to overcome a number of problems. Also, the conductor would need to have an overall Nb_3Sn volume fraction high enough so brittleness would be virtually certain to occur.

Encouraging progress has been made at LLL on developing strain-gage evaluation techniques so sufficient information can be obtained to use in instrumenting coils such as MFTF and for test samples in the tensile tester.

Conductor development for MFTF is now well underway. We have ordered 25-cm-diam sample billets from the four major superconductor manufacturers in the U.S.A. to be processed to the final size: 6.5-mm sq. We will evaluate these conductors and add stabilizing Cu to 2100 m of superconductor, which will then be wound into a test coil. This coil will simulate as closely as possible the conditions expected on MFTF and will enable stability performance to be investigated. The new HFTF cryostat will be used to test this coil together with the first Nb-Ti backing

coils to boost the field at the MFTF conductor close to its maximum value of 7.5 T. Contracts have been placed with Supercon and Airco to develop alternative fabrication processes for adding the required stabilizing Cu cooling surfaces to the MFTF superconducting core.

We continued our development of stress-analysis codes and more refined calculations of the stresses and displacements of the MFTF coil structure. This work was also supported by an independent analysis by the Boeing Aircraft Co. The results of this work confirmed that the proposed structural concept is sound and that the stresses and deflections are acceptable.

ACKNOWLEDGMENTS

The strain-gage work described earlier ("High-Field Cryogenic Tensile-Test Experiment") was a collaborative effort between our group and Henry Freynik and Don Roach of the Materials Engineering Division. Their expertise and hard work were a major factor in the progress to date.

In all of the LLL work, Don Hirzel, Jack Johnston, and Art Rosdahl made significant contributions to the construction, testing, and operation of all the cryogenic facilities.

In particular the authors wish to acknowledge the considerable work of Erna Barr and Larry Gottlieb in the preparation of this report.

REFERENCES

1. M. N. Wilson, Rutherford Laboratory, Chiton-Didcot, England, private communication (August 24, 1976).
2. E. Gregory, W. G. Marancik, and F. T. Ormand, *IEEE Trans. Magn.* MAG-11, 295 (1975).
3. E. Gregory, W. G. Marancik, F. T. Ormand, and J. P. Zbasnik, in *Proc. 5th Int. Conf. Magnet Technology, Rome, Italy, 1975 (MT-5)*, (Laboratori Nazionali del CNEN Servizio Documentazione Frascati, Italy, 1975), p. 301.
4. J. P. Zbasnik, R. R. Vandervoort, C. E. Taylor, D. E. Ping, and D. G. Hirzel, in *Proc. 6vh Symp. Eng. Problems in Fusion Research, San Diego, Calif., 1975* (IEEE Pub. #75CH1097-5-NPS, Piscataway, New Jersey, 1976), p. 101.
5. D. N. Cornish, A. R. Harvey, R. L. Nelson, C. E. Taylor, and J. P. Zbasnik, *Superconducting Magnet Development Program Progress Report*, Lawrence Livermore Laboratory, Livermore, Calif., UCRL-50031-75 (1975).
6. D. N. Cornish, D. W. Deis, R. L. Nelson, R. M. Scanlan, C. E. Taylor, R. R. Vandervoort, F. J. Wittmayer, and J. P. Zbasnik, *IEEE Trans.* MAG-13, 454 (1977).
7. J. P. Zbasnik, R. L. Nelson, D. N. Cornish, and C. E. Taylor, *Advances in Cryogenic Eng.* 22, K. E. Timmerhaus, Ed. (Plenum Press, New York, 1976), p. 370.
8. C. F. Old and J. P. Charlesworth, *Cryogenics* 16, 469 (1976).
9. Y. Hashimoto, K. Yoshizaki, and M. Tanaka, in *Proc. 5th Int. Cryo. Eng. Conf., Kyoto, 1974* (IPC Science and Technology Press, London, 1974).
10. P. W. Bridgeman, *Studies in Large Plastic Flow and Fracture* (McGraw-Hill, New York, 1952).
11. B. Avitzur, *Metal Forming: Processes and Analysis* (McGraw-Hill, New York, 1972).
12. ASEA, *"Quintus, Hydrostatic Extrusion Press Type Q. E."*, Sweden, Pamphlet AQ14-102E.
13. J. B. Pfeffer, *Hydrostatic Extrusion — Now a Production Process*, Society of Manufacturing Engineers, Philadelphia, Pa, Technical Paper MF74-209 (1974).
14. A. R. Bobrowsky, "Augmented Hydrostatic Extrusion," presented at *Mfg. of Wire Conf. of Soc. Mfg. Engrs., Philadelphia, Pa, 1976.*

15. J. M. Alexander and B. Lengyel, *Hydrostatic Extrusion* (Mills and Boon, London, 1975).
16. P. Andrus and G. Schmehl, "Western Electric Company Continuous Hydrostatic Wire Extrusion," presented at *Mfg. of Wire Conf. of Soc. Mgf. Engrs., Philadelphia, Pa, 1976.*
17. T. Altan and S. Kobayashi, *ASME Trans., Series B* 90, 107 (1968).
18. R. M. Guha and B. Lengyel, *J. Inst. Eng. (India), Mech. Eng. Div.* 54, 117 (1974).
19. A. R. E. Singer and S. H. K. Al-Samarrai, *J. Inst. Metals* 89, 225 (1974).
20. M. Suenaga, O. Horigami, and T. S. Lubman, *Appl. Phys. Lett.* 25, 624 (1974).
21. M. Hansen, *Constitution of Binary Alloys* (McGraw-Hill, New York, 1958).
22. J. A. Lee, C. F. Olds, and D. Larbalestier, *Physique sous Champs Magnetique Intenses*, Colloques Internationaux, Paris, CNRS No. 242 (1974).
23. V. Zwicker and L. Rinderer, *Z. Metallkd.* 66, 739 (1975).
24. I. Kawakatsu, T. O. Osawa, and H. Yanaguchi, *Trans. T.I.M.* 13, 436 (1972).
25. H. Oikawa and A. Hosoi, *Scripta Metallurgica* 9, 823 (1975).
26. W. H. McAdams, W. F. Kennel, C. S. Minden, C. Rudolf, C. Picornell, and J. E. Dow, *Ind. Eng. Chem.* 41, (1945).
27. J. C. Telinde, Douglas Aircraft, Huntington Beach, Calif., Paper No. 3835 (1966).
28. D. N. Cornish, A. R. Harvey, R. L. Nelson, C. E. Taylor, and J. P. Zbasnik, *High-Field Test Facility Major Project Proposal,* Lawrence Livermore Laboratory, Livermore, Calif., LLL-Prop-130 (1975).

PUBLICATIONS

Proceedings of the Sixth Symposium on Engineering Problems of Fusion Research, San Diego, Calif., November 1975

J. P. Zbasnik, R. R. Vandervoort, C. E. Taylor, D. E. Ping, and D. G. Hirzel, "Tests on Multifilamentary Nb_3Sn Superconductors," p. 101.

D. N. Cornish, J. P. Zbasnik, and H. E. Pattee, "Explosive Joints in Nb-Ti/Cu Composite Superconductors," p. 106.

A. R. Harvey and J. A. Rinde, "Electrical Insulation for Large Multiaxis Superconducting Magnets," p. 606.

S. J. Sackett, "Calculation of Electromagnetic Fields and Forces in Coil Systems of Arbitrary Geometry," p. 935.

Proceedings of the 1976 Applied Superconductivity Conference, Stanford, Calif., August 1976

R. H. Bulmer, M. O. Calderon, D. N. Cornish, T. A. Kozman, and S. J. Sackett, "The MX Magnet System," to be published (1976).

D. W. Deis, "Multifilament Nb_3Sn Conductors: Progress and Prospects," to be published (1976).

D. N. Cornish, D. W. Deis, R. L. Nelson, R. M. Scanlan, C. E. Taylor, R. R. Vandervoort, F. J. Wittmayer, and J. P. Zbasnik, "Development of Multifilamentary Nb_3Sn Conductors for Fusion Research," to be published (1976).

Proceedings of the Second International Conference on Mechanical Behavior of Materials, Boston, Mass., August 1976

S. J. Sackett, J. M. Kelly, and P. P. Gillis, "A Probabilistic Approach to Polycrystalline Plasticity," II, p. 28.

Proposal

D. N. Cornish, A. R. Harvey, R. L. Nelson, C. E. Taylor, and J. P. Zbasnik, *High-Field Test Facility Major Project Proposal* Lawrence Livermore Laboratory, Livermore, Calif., LLL-Prop-130 (1975).

LG
GPO 789-086/4936